THE JOURNAL OF PHYSICAL CHEMISTRY B

Article

pubs.acs.org/JPCB

Carbon Relaxation in $^{13}C^{\alpha}-H^{\alpha}$ and $^{13}C^{\alpha}-D^{\alpha}$ Spin Pairs as a Probe of Backbone Dynamics in Proteins

Hechao Sun,[†] Dong Long,[‡] Rafael Brüschweiler,[‡] and Vitali Tugarinov*[,†]

[†]Department of Chemistry and Biochemistry, University of Maryland, College Park, Maryland 20742, United States

[‡]Chemical Sciences Laboratory, Department of Chemistry and Biochemistry and the National High Magnetic Field Laboratory, Florida State University, Tallahassee, Florida 32306, United States

Supporting Information

ABSTRACT: NMR methodology for the measurements of α-carbon R_1 and $R_{1\rho}$ spin relaxation rates in $^{13}C^{\alpha}-H^{\alpha}$ and $^{13}C^{\alpha}-D^{\alpha}$ spin pairs of U-[^{13}C; ^{15}N] partially deuterated proteins is developed. The *intra*-HN[CA] NMR experiment isolates carbon nuclei belonging to either $^{13}C^{\alpha}-H^{\alpha}$ or $^{13}C^{\alpha}-D^{\alpha}$ spin systems in the same protein sample prior to the measurement of $^{13}C^{\alpha}$ relaxation rates. The differences between R_1 and R_2 rates in the two spin pairs (ΔR_1, ΔR_2) eliminate all contributions to $^{13}C^{\alpha}$ decay rates not associated with direct $^{13}C^{\alpha}-^{1}H^{\alpha}(D^{\alpha})$ dipolar interactions including chemical exchange and serve as robust measures of $C^{\alpha}-H^{\alpha}(D^{\alpha})$ bond vector motions in proteins. The methodology is applied to the relaxation study of α-carbon sites in the protein ubiquitin at two temperatures. The measures of order of individual $C^{\alpha}-H^{\alpha}(D^{\alpha})$ bond vectors (S^2) in ubiquitin derived from the fitting of differential rates (ΔR_1, ΔR_2) unambiguously report on protein dynamics, thereby eliminating potential contributions from modulations of $C^{\alpha}-H^{\alpha}(D^{\alpha})$ bond lengths by their environment. They are comparable to the ones obtained from a molecular dynamics simulation at 27 °C.

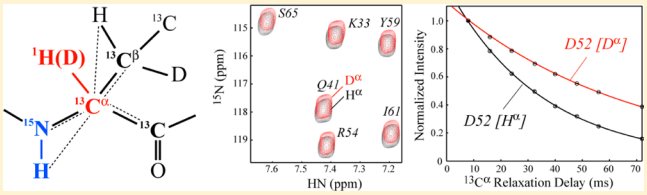

INTRODUCTION

Since the first demonstration of ^{13}C line narrowing in uniformly [^{15}N; ^{13}C]-labeled proteins achieved via perdeuteration in combination with ^{2}H-decoupling two decades ago,[1] deuteration has emerged as an important tool for solution NMR studies of high-molecular-weight proteins.[2−5] Apart from direct effects of deuteration on ^{13}C line widths due to slower relaxation rates of carbons attached to deuterons,[6,7] it is widely recognized that transverse relaxation optimized spectroscopy (TROSY)[8,9] benefits from deuteration of protein molecules. TROSY effects in $^{1}H-^{15}N$ spin systems of backbone amides,[8,10] aromatic $^{1}H-^{13}C$ moieties,[11] and $^{13}CH_2$ groups of proteins[12] are significantly enhanced when the protons that are not directly detected in NMR experiments are substituted for deuterons. Deuteration is of paramount importance for methyl-TROSY of selectively protonated $^{13}CH_3$ groups,[13,14] where the line widths of the slow-relaxing components of methyl $^{1}H-^{13}C$ multiple-quantum coherences are directly dependent on the deuteration levels of the rest of the protein molecule.[13,15,16]

Quantitative evaluation of the effects of deuteration on several NMR parameters in proteins has been reported: one bond $^{1}H-^{13}C$ scalar couplings in methyl groups,[17] equilibrium proton/deuterium fractionation factors for backbone amides,[18] deuterium isotope shifts of different nuclei in proteins,[19−24] as well as the relaxation properties of backbone amide ^{15}N nuclei in $^{15}N-D$ spin pairs quantified via direct nitrogen detection[25] or (indirect) HA(CACO)N-based techniques.[26] Very recently, we have described a set of precision NMR measurements of deuterium isotope effects on the chemical shifts of ^{1}HN, ^{15}N, ^{13}CO, and $^{13}C^{\alpha}$ nuclei in the partially (60%) deuterated protein ubiquitin and correlated these shifts with the protein backbone geometry.[27] Even though ^{13}C relaxation studies of biomacromolecules have a three decade long history,[28−35] to the best of our knowledge, quantitative assessment of the utility of $^{13}C^{\alpha}-D^{\alpha}$ spin pairs for the description of protein backbone dynamics in proteins is still lacking.

Here, we describe accurate NMR measurements of carbon R_1 and $R_{1\rho}$ spin relaxation rates in $^{13}C^{\alpha}-H^{\alpha}$ and $^{13}C^{\alpha}-D^{\alpha}$ spin pairs of U-[^{13}C;^{15}N] proteins partially deuterated at carbon-α sites. Partial deuteration at α positions allows the developed 2D *intra*-HN[CA] NMR experiment(s) whereby either $^{13}C^{\alpha}-H^{\alpha}$ or $^{13}C^{\alpha}-D^{\alpha}$ spin systems are isolated and selected prior to the measurement of $^{13}C^{\alpha}$ decay rates, to be applied to the spin systems of both varieties in the same protein sample. The differences between R_1 and R_2 rates in the two spin pairs (ΔR_1, ΔR_2) are devoid of any "external" contributions to $^{13}C^{\alpha}$ relaxation rates, such as dipolar homonuclear $^{13}C-^{13}C$ and heteronuclear $^{13}C-^{15}N$, the interactions of ^{13}C with external (non-H^{α}) ^{1}H spins, $^{13}C^{\alpha}$ chemical shift anisotropy (CSA) relaxation, and chemical exchange, and, as such, serve as reliable measures of $^{13}C^{\alpha}-H^{\alpha}(D^{\alpha})$ bond vectors dynamics in proteins. The parameters of local dynamics derived from differential $^{13}C^{\alpha}$ R_1 and R_2 rates in the protein ubiquitin at two temperatures (27 and 10 °C) under the assumption that local dynamics is not

Received: December 13, 2012
Revised: January 9, 2013
Published: January 11, 2013

   dx.doi.org/10.1021/jp312292k | *J. Phys. Chem. B* 2013, 117, 1308−1320

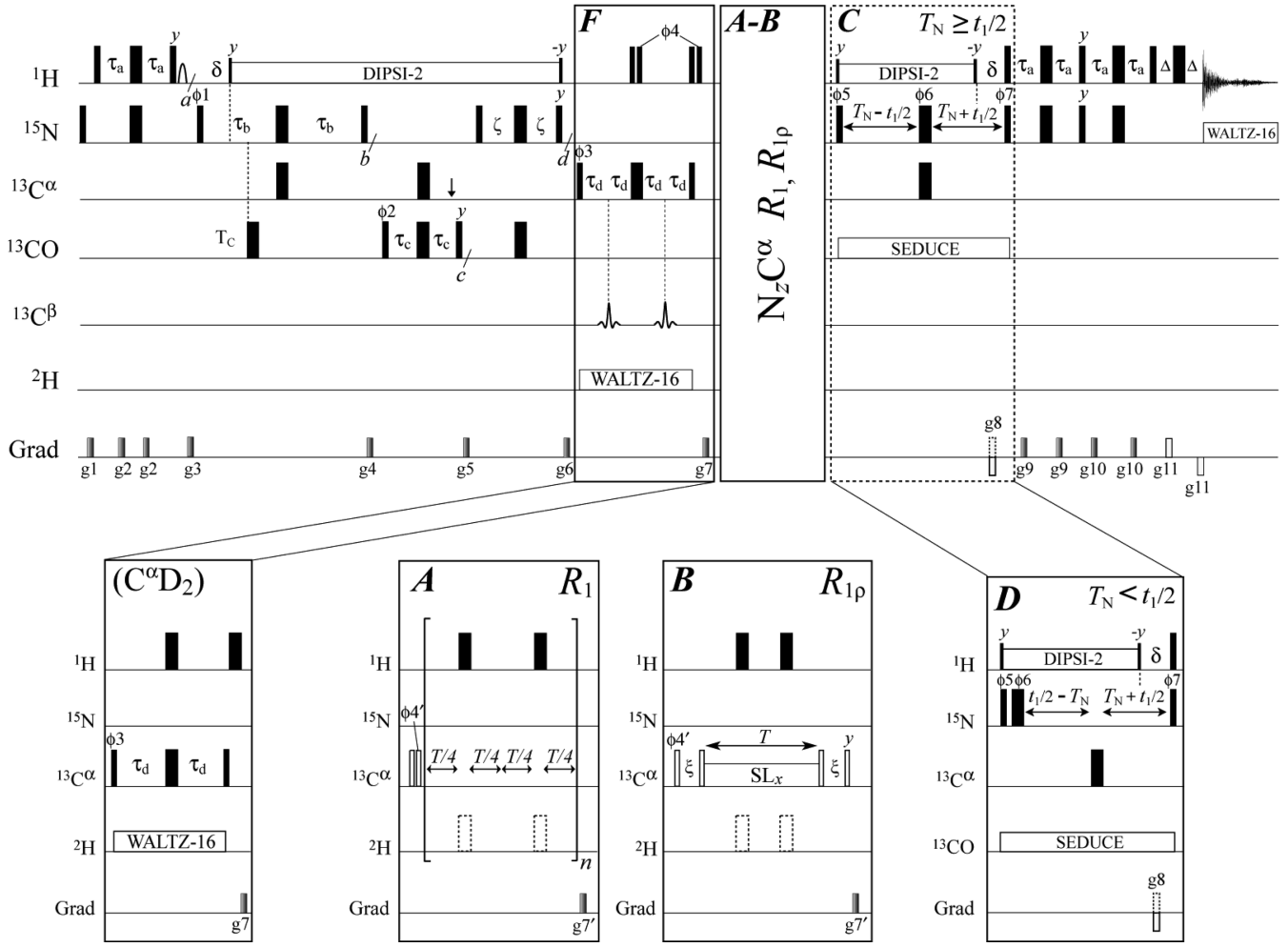

Figure 1. 2D *intra*-HN[CA] pulse scheme for the measurement of $^{13}C^\alpha$ relaxation rates in $^{13}C^\alpha$–H^α and $^{13}C^\alpha$–D^α spin pairs. See Materials and Methods for experimental details.

affected by proton-to-deuterium substitution at α sites are compared to their counterparts derived from the measurements of $^{13}C^\alpha$ R_1 and R_2 rates in the protonated sample of the protein selectively enriched with ^{13}C at α-carbon sites, [$^{13}C^\alpha$]-labeled ubiquitin.[36,37]

MATERIALS AND METHODS

NMR Samples. Three samples of wild-type human ubiquitin have been used in this work: (i) U-[^{15}N; ^{13}C]-labeled ubiquitin ~60% deuterated at α-carbon positions; this deuteration level at aliphatic carbon sites is achieved by the use of U-[^{13}C]-glucose as the main carbon source along with 60% D_2O/40% H_2O M9 minimal medium;[27] (ii) [$^{13}C^\alpha$]-labeled ubiquitin obtained via the use of [2-$^{13}C_1$]-labeled glucose as the principal carbon source during protein production;[36,37] this labeling strategy provides a protein selectively ^{13}C-labeled at all C^α sites except Leucines with varying degrees of ^{13}C incorporation;[36] and (iii) U-[^{15}N; ^{13}C]-labeled fully protonated sample of ubiquitin. The U-[^{15}N,^{13}C, 60%-^2H/40%-^1H]-labeled NMR sample was 3.0 mM, while the [$^{13}C^\alpha$]-labeled and the protonated U-[^{15}N; ^{13}C]-labeled samples were 2.5 mM in protein concentration. All the samples were dissolved in a 20 mM 90% H_2O/10% D_2O sodium phosphate buffer (pH 6.8) containing 0.03% NaN_3 and a set of protease inhibitors.

Experimental NMR Details. Figure 1 shows the two-dimensional (2D) *intra*-HN[CA] pulse scheme that has been designed for the measurements of $^{13}C^\alpha$ relaxation rates in $^{13}C^\alpha$–H^α and $^{13}C^\alpha$–D^α spin pairs of U-[^{13}C]-labeled proteins. A series of 2D data sets providing the correlations at ($\omega_{HN,i}$; $\omega_{N,i}$) chemical shifts are recorded with the parametrically varied T delays for the measurements of R_1 (inset ***A***) and $R_{1\rho}$ (inset ***B***) rates in $^{13}C^\alpha$–H^α/$^{13}C^\alpha$–D^α spin pairs. The BIRD[38,39] filtering element ***F*** ensures the selection for molecular species with either $^{13}C^\alpha$–H^α or $^{13}C^\alpha$-D^α spin pairs resulting in the two subseries of R_1 and $R_{1\rho}$ relaxation data. The element labeled "$C^\alpha D_2$" in Figure 1 is employed for selection of $^{13}C^\alpha D_2$ groups in glycine residues and is used instead of the element ***F*** when $^{13}C^\alpha$–D^α selection is employed. Inset ***D*** shows the part of the scheme enclosed in ***C*** that can be used for longer t_1 acquisition times ($t_1 > 2T_N$).

All narrow(wide) rectangular pulses in Figure 1 are applied with the flip angles of 90°(180°) along the *x*-axis unless indicated otherwise. The $^1H(^2H;^{15}N)$ carriers are positioned at 4.7(4.0;119) ppm. The ^{13}C carrier is placed at 57 ppm, switched to 176 ppm before the first 90° ^{13}CO pulse (after the gradient g4), and subsequently returned to 57 ppm after the gradient g6. All ^1H and ^{15}N pulses are applied with maximum possible power, while the ^1H pulse shown with an arc (preceding the gradient g3) is implemented as a water-selective 1.4 ms pulse of rectangular shape. All 90°(180°) $^{13}C_\alpha$ and ^{13}CO pulses shown with filled

dx.doi.org/10.1021/jp312292k | J. Phys. Chem. B 2013, 117, 1308–1320

rectangles are applied with a field strength of $\Delta/\sqrt{15}(\Delta/\sqrt{3})$ where Δ is the difference (in Hz) between $^{13}C_\alpha$ and ^{13}CO chemical shifts,[40] while the $^{13}C_\alpha$ in insets ***A*** and ***B*** shown with open rectangles are applied with maximum possible power. The vertical arrow at the end of the $2\tau_c$ period indicates the position of the $^{13}C_\alpha$ Bloch−Siegert shift compensation pulse.[40] $^{13}C_\beta$-shaped pulses in the middle of $2\tau_d$ periods are 1.52 ms I-BURP2[41] pulses centered at 30 ppm by phase modulation of the carrier[42,43] (inversion bandwidth of 17 ppm at 600 MHz). ^2H 180° pulses shown with dashed rectangles in insets ***A*** and ***B*** are optional and intended to remove the effects of $^{13}C^\alpha$ CSA/$^{13}C^\alpha$−D^α dipolar cross-correlated relaxation. In practice, inclusion of these pulses does not affect the extracted $R_{1\rho}$ and R_1 relaxation rates in $^{13}C^\alpha$−D^α spin pairs to within experimental errors. ^{15}N WALTZ-16[44] decoupling during acquisition is achieved using a 1.25-kHz field, while ^2H WALTZ-16 decoupling uses a 0.9 kHz field. ^1H DIPSI-2[45] decoupling is applied with 7.5 kHz power. SEDUCE[46] ^{13}CO decoupling is implemented with 300 μs seduce-shaped pulses applied at ^{13}CO frequency by phase modulation of the carrier.[42,43] The purpose of the second pair of 90°$_{\phi4}$−90° ^1H pulses inside the filtering element ***F*** is to return the water magnetization to the state prior to the element ***F***. The spin-lock field of 2 kHz was applied along the x axis for all $R_{1\rho}$ measurements (SL_x; inset ***B***). Delays are: τ_a = 2.7 ms; τ_b = 25 ms; τ_c = 4.5 ms; ζ = 15 ms ($\sim 1/4^1J_{NC'}$); τ_d = 1.75 ms; T_N = 13 ms; T_C = 16 ms; δ = 5.4 ms; Δ = 400 μs. Delay ξ (inset ***B***) is equal to $1/(2\pi\nu_1) - (4/\pi)pw_c$, where ν_1 is the strength (in Hz) of the spin-lock field and pw_c is the width of the $^{13}C_{\phi4'}$ pulse.[33] The phase cycle is: $\phi1 = x,-x$; $\phi2 = 2(x),2(-x)$; $\phi3 = 4(x),4(-)$; $\phi4 = 8(x),8(-x)$; $\phi4' = 16(x),16(-x)$ for R_1 measurements (inset ***A***), while $\phi4' = 16(y),16(-y)$ for $R_{1\rho}$ measurements (inset ***B***); $\phi5 = x$; $\phi6 = 16(x),16(-x)$; $\phi7 = x$; rec. = $x,-x,-x,x,-x,x,x,-x$, $2(-x,x,x,-x, x,-x,-x,x)$, $x,-x,-x,x, -x,x,x,-x$ for selection of $^{13}C^\alpha$−H^α, and rec. = $2(x,-x,-x,x,-x,x,x,-x)$, $2(-x,x,x,-x,x,-x,-x,x)$ for selection of $^{13}C^\alpha$−D^α spin pairs. When the element "$C^\alpha D_2$" is employed for selection of $^{13}C^\alpha D_2$ groups in glycines, the pulses with the phase $\phi4$ are not applied, and the receiver phase remains the same as for the $^{13}C^\alpha$−D^α filtering above. Quadrature detection in t_1 is achieved via the Rance−Kay sensitivity enhancement scheme: for each t_1 value a pair of spectra is recorded with ($\phi7 = x$; g8) and ($\phi7 = -x$; −g8) and manipulated postacquisition.[47,48] The phase $\phi5$ is inverted for each t_1 point.[49] Durations and strengths of pulsed-field gradients in units of (ms; G/cm) are: g1 = (1; 20); g2 = (0.25; 5); g3 = (1.2; 15); g4 = (1.0; 12); g5 = (0.6; 10); g6 = (0.8; 8); g7 = (0.75; 15); g7′ = (0.7; 20); g8 = (1.25; −20); g9 = (0.4; 15); g10 = (0.5; 12); g11 = (0.0625; 20).

In the measurements of R_1 rates of both spin pair types (inset ***A***; Figure 1), relaxation T delays have been restricted to multiples of 40 ms, with the spacing between the two adjacent ^1H 180° pulses of 20 ms. We found this rate of ^1H pulsing during T delays sufficient for elimination of $^{13}C^\alpha$ CSA/$^{13}C^\alpha$−H^α dipolar and ^{13}C−^{13}C/^{13}C−^1H dipole−dipole cross-correlated relaxation effects.[33,50−52] Faster ^1H pulsing during T delays did not lead to statistically significant (beyond experimental error) changes in the extracted R_1 rates of ubiquitin at both 27 and 10 °C. In the measurements of $R_{1\rho}$ rates (inset ***B***; Figure 1), the application of only one pair of ^1H 180° pulses during the spin-lock duration T was found sufficient for elimination of $^{13}C^\alpha$ CSA/$^{13}C^\alpha$−H^α dipolar and ^{13}C−^{13}C/^{13}C−^1H dipole−dipole cross-correlations. Much faster ^1H pulsing during T delays in $R_{1\rho}$ experiments resulted in a small but statistically significant systematic increase of 2 to 2.5% in the extracted $R_{1\rho}$ rates at both temperatures, in agreement with previous observations.[53]

NMR Measurements and Data Analysis. All NMR measurements were performed on a 600 MHz Bruker Avance III spectrometer equipped with a room-temperature triple-resonance z-gradient probe. Each *intra*-HN[CA] 2D data set in R_1, $R_{1\rho}$ relaxation series recorded with the pulse scheme of Figure 1 comprised [512, 44] complex points in the corresponding dimensions of the [^{1}HN,^{15}N] correlation maps, with the respective acquisition times of [64, 26] ms. Usually, a recovery delay of 1.5 s was used along with 64 scans/FID giving rise to the net acquisition time of ∼2.5 h/experiment. Separate R_1, $R_{1\rho}$ relaxation series have been acquired for selection of $^{13}C^\alpha HD$ and $^{13}C^\alpha D_2$ groups of glycines, with the ^{13}C carrier placed at 46 ppm and the spin-lock field strength and other acquisition parameters as specified above. Typically, the relaxation T delays in R_1 measurements in both spin pairs have been restricted to multiples of 40 ms, while the spin-lock duration T's in $R_{1\rho}$ measurements have been restricted to multiples of 8 ms.

$^{13}C^\alpha$ R_1, $R_{1\rho}$ rates in the fully protonated U-[^{15}N; ^{13}C]-labeled sample of ubiquitin have been quantified via recording of a series of [$^1H^\alpha$,$^{13}C^\alpha$] correlation maps using slight modifications of the experiments developed earlier by Yamazaki, Muhandiram, and Kay,[33] with the main acquisition parameters identical to those used for the *intra*-HN[CA] scheme in Figure 1. $^{13}C^\alpha$ R_1, $R_{1\rho}$ rates in the selectively [$^{13}C^\alpha$]-labeled sample have been measured using the same pulse schemes[33] but without constant-time ^{13}C evolution in t_1. Thus obtained R_1 and $R_{1\rho}$ rates at 27 °C proved practically indistinguishable to within random errors from the same rates quantified earlier in the [$^{13}C^\alpha$]-labeled ubiquitin using the gradient sensitivity-enhanced experiments.[37]

All NMR spectra were processed using the NMRPipe/NMRDraw program[54] and associated software. $^{13}C^\alpha$ relaxation rates were obtained by fitting peak intensities to a single exponential function of the form $I = I_0 \exp(-RT)$, where I is the measured intensity and R is the relaxation rate. Errors in peak intensities have been estimated from duplicate measurements or from the noise-floor level of the spectra, whichever the highest, and subsequently propagated to the errors in the extracted rates using Monte Carlo analysis.[55] R_2 rates have been extracted from the $R_{1\rho}$ rates using the relationship

$$R_2 = \left(\frac{1}{\sin^2\theta}\right)[R_{1\rho} - R_1\cos^2\theta] \quad (1)$$

where the angle $\theta = \tan^{-1}(\omega_1/\Omega)$, where ω_1 denotes the RF field strength of the ^{13}C spin-lock and Ω the offset from the ^{13}C carrier. The offsets Ω in $^{13}C^\alpha$−D^α spin pairs have been calculated taking into account one-bond deuterium isotope shifts of $^{13}C^\alpha$ nuclei established previously.[27] The average random uncertainties in R_1 and R_2 rates in the relaxation series obtained using the scheme of Figure 1 are 1.1(1.5)% in $^{13}C^\alpha$−D^α($^{13}C^\alpha$−H^α) spin pairs at 27 °C and 1.5(2.0)% at 10 °C. Random errors in the differences of ^{13}C R_1 and R_2 rates between the two spin pairs, $\Delta R_1 = R_1[^{13}C^\alpha$−$H^\alpha] - R_1[^{13}C^\alpha$−$D^\alpha]$ and $\Delta R_2 = R_2[^{13}C^\alpha$−$H^\alpha] - R_2[^{13}C^\alpha$−$D^\alpha]$, were propagated from the errors in individual rates using standard error propagation rules.[56]

The expressions for relaxation rates used in this work derive from the standard formulas for dipolar relaxation rates in two-spin X−^{1}H/X−D systems.[32,57] The following form of the spectral density function for an axially symmetric orientational molecular diffusion tensor[58−60] was used in all calculations

$$J(\omega) = S^2\left(\frac{A_1\tau_1}{1+(\omega\tau_1)^2} + \frac{A_2\tau_2}{1+(\omega\tau_2)^2} + \frac{A_3\tau_3}{1+(\omega\tau_3)^2}\right) + (1-S^2)\frac{\tau'}{1+(\omega\tau')^2} \quad (2)$$

where S^2 is the generalized order parameter squared describing the fluctuations of C^α–$H^\alpha(D^\alpha)$ bond vectors; $A_1 = (3/4)\sin^4(\beta)$; $A_2 = 3\sin^2(\beta)\cos^2(\beta)$; $A_3 = [(3/2)\cos^2(\beta) - 0.5]^2$; $\tau_1 = (4D_\parallel + 2D_\perp)^{-1}$; $\tau_2 = (D_\parallel + 5D_\perp)^{-1}$; $\tau_3 = (6D_\perp)^{-1}$; $D_\parallel$ and $D_\perp$ are the parallel and perpendicular components of the molecular diffusion tensor; β is the angle between the C^α–$H^\alpha(D^\alpha)$ bond vector and the unique diffusion axis; and $1/\tau' = 1/\tau_f + 1/\tau_{c,eff}$, where the effective correlation time of overall rotation $\tau_{c,eff} = (2D_\parallel + 4D_\perp)^{-1}$ and τ_f is the correlation time of fast local motions. Direction cosines for C^α–$H^\alpha(D^\alpha)$ bond vectors of human ubiquitin have been obtained from the protonated crystal structure of ubiquitin (PDB code 1ubq[61]). The values of $\tau_{c,eff}$ = 4.16(6.92) ns were used for ubiquitin at 27(10) °C as determined from ^{15}N relaxation measurements at these temperatures previously,[62] with $D_\parallel/D_\perp$ = 1.18, and the polar angles which determine the orientation of the unique axis of the global diffusion tensor in the inertial coordinate frame, $\theta = 8°$ and $\phi = -16°$, assumed to be invariant with temperature. Because the filtering elements employed in the scheme of Figure 1 do not permit the differentiation between individual protons/deuterons of $^{13}C^\alpha$–HD and $^{13}C^\alpha$–D_2 moieties of glycines, the ΔR_1 and ΔR_2 rates in these cases have been interpreted based on an isotropic spectral density function.

Deuteration leads to a slight decrease in the effective length of C–H bonds.[63] While the C^α–H^α distance (r_{CH}) of 1.10 Å[33,64] was used for all calculations in this work, the value for C^α–D^α distance (r_{CD}) is assumed to be 0.005 Å lower, 1.095 Å.[63] The C^α–C^β and C^α–C' internuclear distances (r_{CC}) were assumed to be equal to 1.53 Å,[33,65] while the distance between C^α and backbone nitrogen N (r_{CN}) of 1.45 Å[33,66,67] was used. The average N–$H^\alpha(D^\alpha)$ internuclear distance of 2.10 Å has been measured from the structure of (protonated) ubiquitin. A uniform value of 25 ppm[68,69] was used for the (assumed axially symmetric) CSA of $^{13}C^\alpha$ spins in all calculations.

Molecular Dynamics Simulations. Molecular dynamics (MD) trajectories (500 ns) of ubiquitin at 27 °C were generated as described previously,[70,71] using the GROMACS software package[72] with TIP3P explicit water model[73] and the ff99SB_φ–ψ(g24,CS)[74] force field.

RESULTS AND DISCUSSION

Transverse and Longitudinal Spin Relaxation Rates of α-Carbons in Proteins. Whereas in ^{15}N relaxation studies of protein backbone dynamics, amide ^{15}N–^{1}H bond vectors can commonly be treated as isolated spin pairs, relaxation of α-carbons in U-[^{13}C]-labeled proteins involves taking into account many additional relaxation pathways extraneous to the (direct) dipolar interaction between $^{13}C^\alpha$ and $^1H^\alpha$ spins.[33,75,76] In U-[^{13}C;^{15}N]-labeled and protonated protein samples, these include dipolar interactions of $^{13}C^\alpha$ nuclei with (i) directly bonded ^{13}C spins ($^{13}C^\beta$ and carbonyls, $^{13}C'$), (ii) ^{15}N nuclei, and (iii) external proton spins—mainly ^{1}HN (for samples dissolved in H_2O) and $^1H^\beta$ protons. Schematic representation of a dipeptide fragment in various states of protonation/deuteration at aliphatic carbon positions is shown in Figure 2, with the auto- and cross-relaxation contributions to $^{13}C^\alpha$ decay indicated beside each bond vector connecting the contributing nuclei. By far the most significant is

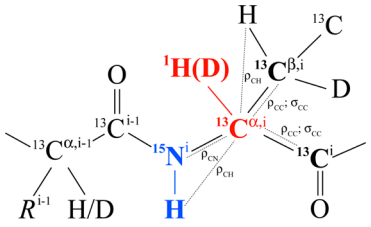

Figure 2. Schematic representation of a dipeptide fragment in various states of protonation/deuteration at aliphatic carbon positions. The spin pairs whose relaxation parameters are measured, $^{13}C^\alpha$–$H^\alpha(D^\alpha)$, are shown in red, while the nuclei whose chemical shifts are evolved (^{1}H; ^{15}N) are shown in blue. The auto(ρ)- and cross(σ)-relaxation contributions to $^{13}C^\alpha$ decay are indicated on the figure.

the contribution of homonuclear $^{13}C^\alpha$–$^{13}C^\beta$ and $^{13}C^\alpha$–$^{13}C'$ dipolar interactions to $^{13}C^\alpha$ longitudinal decay rates (R_1) since unlike the $^{13}C^\alpha$ R_1 relaxation rates in isolated $^{13}C^\alpha$–$^1H^\alpha(D^\alpha)$ spin pairs these contributions have components proportional to the spectral density evaluated at zero frequency, $J(0)$.[33,75,76] The labeling strategy that allows selective ^{13}C incorporation into α-carbon sites of proteins developed by Lundström et al.[36] eliminates homonuclear ^{13}C–^{13}C dipolar couplings. Figure 3 shows $^{13}C^\alpha$ relaxation rates measured in ubiquitin with different ^{13}C isotope labeling schemes (see Materials and Methods): R_1, R_2 rates in the U-[^{13}C]- and selectively [$^{13}C^\alpha$]-labeled samples at 27 °C (Figure 3a,b) and the same rates obtained at 10 °C (Figure 3c,d). $^{13}C^\alpha$ R_1 rates are uniformly higher in the U-[^{13}C]-sample by 10.5(22.1)% on average at 27(10) °C (Figure 3a,c), while R_2 rates are affected to a much smaller extent but are higher on average by 4.2% at both temperatures (Figure 3a,c). These results are in good agreement with rate calculations that take into account possible ^{13}C–^{13}C dipolar interactions: 9.9(22.6)% increase in R_1 and 2.1(2.1)% increase in R_2 predicted in U-[^{13}C]-samples at 27(10) °C using a set of local dynamics parameters ($S^2 = 0.9$; $\tau_f = 20$ ps) (see Figure S1 of the Supporting Information for the comparison of calculated $^{13}C^\alpha$ auto-(R_1, R_2) and cross-(σ)-relaxation rates for U-[^{13}C]-labeled and selectively [$^{13}C^\alpha$]-labeled proteins).

Clearly, the relative proportion of all the contributions listed above (i–iii) to the total relaxation rate increases upon substitution of a proton for a deuteron at α sites. We estimate that in ubiquitin at 27 °C the fraction of the total, cumulative $^{13}C^\alpha$ R_1 and R_2 rates due to the (direct) $^{13}C^\alpha$–$^1H^\alpha$ dipolar relaxation in $^{13}C^\alpha$–$^1H^\alpha$ spin pairs is ~83% and ~90%, respectively. In $^{13}C^\alpha$–D^α spin pairs, these fractions decrease, respectively, to 53% and 49%. In ubiquitin at 10 °C, the contribution of the $^{13}C^\alpha$–$^1H^\alpha$($^{13}C^\alpha$–D^α) dipolar relaxation to the total R_1 and R_2 decay rates drops to ~74(41)% and ~90(46)%, respectively. Of note, in contrast to the CSA of backbone ^{15}N nuclei in proteins,[77–80] $^{13}C^\alpha$ CSA is small[32,75,76] and very variable.[81,82] It can affect appreciably only R_2 rates in $^{13}C^\alpha$–D^α spin pairs where the dipolar contribution to the total relaxation rate is reduced (respective calculated contributions of 4% and 5.5% of the total $^{13}C^\alpha$ R_2 at 27 and 10 °C for the CSA of 25 ppm at 600 MHz).

Although selective [$^{13}C^\alpha$]-labeling eliminates ^{13}C–^{13}C dipolar couplings as well as the possibility of Hartmann–Hahn magnetization transfer[83] during $R_{1\rho}$ measurements, the incorporation of ^{13}C into α positions is only 40% at the best, with Leucine residues remaining unlabeled.[36] The remaining dipolar interactions (^{13}C–^{15}N, external ^{13}C–^{1}H), small but highly variable $^{13}C^\alpha$ CSA, and possible contributions to R_2 rates due to chemical exchange have to be considered when $^{13}C^\alpha$ spin

dx.doi.org/10.1021/jp312292k | J. Phys. Chem. B 2013, 117, 1308–1320

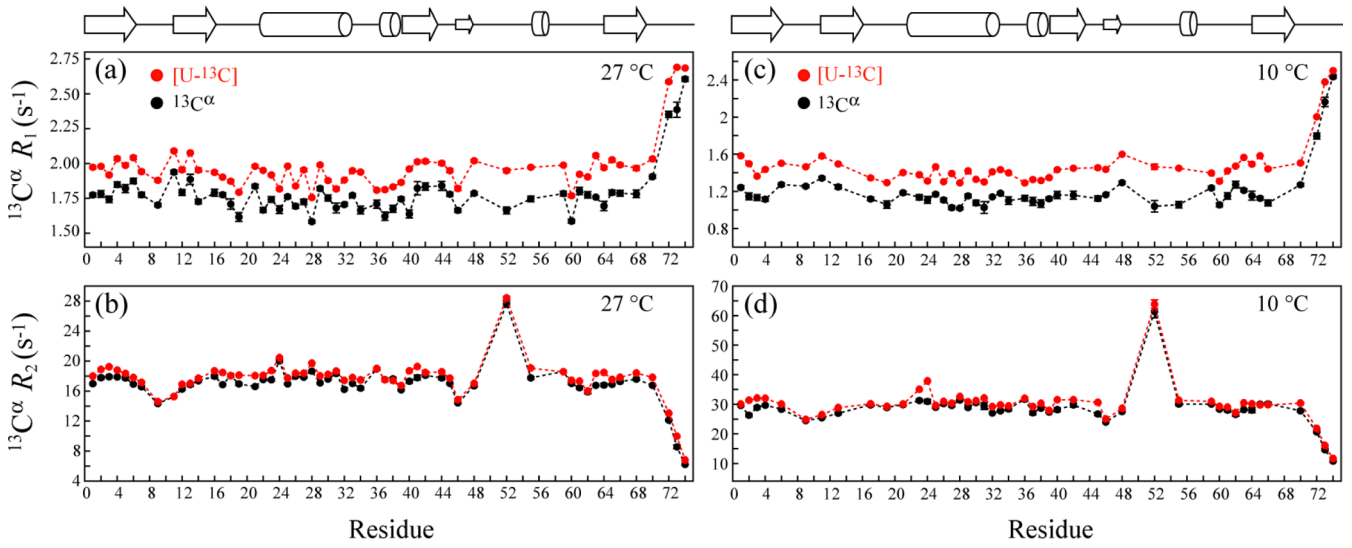

Figure 3. $^{13}C^{\alpha}$ relaxation rates (s^{-1}) measured in ubiquitin with different ^{13}C isotope labeling schemes, plotted as a function of residue numbers: (a) $^{13}C^{\alpha}$ R_1 and (b) $^{13}C^{\alpha}$ R_2 measured in the U-[^{13}C]- (red circles) and selectively [$^{13}C^{\alpha}$]-labeled (black circles) ubiquitin at 27 °C; (c) $^{13}C^{\alpha}$ R_1 and (d) $^{13}C^{\alpha}$ R_2 color-coded as in (a,b) obtained at 10 °C. The plots are drawn for the same subset of residues in both types of samples. Leucine residues are excluded from the plots as leucines have only residual $^{13}C^{\alpha}$-labeling when [2-$^{13}C_1$]-glucose is used as the principal carbon source during protein production.[36] Schematic diagram of the secondary structure of the protein is shown above the figure with arrows and cylinders denoting β-strands and helical regions, respectively.

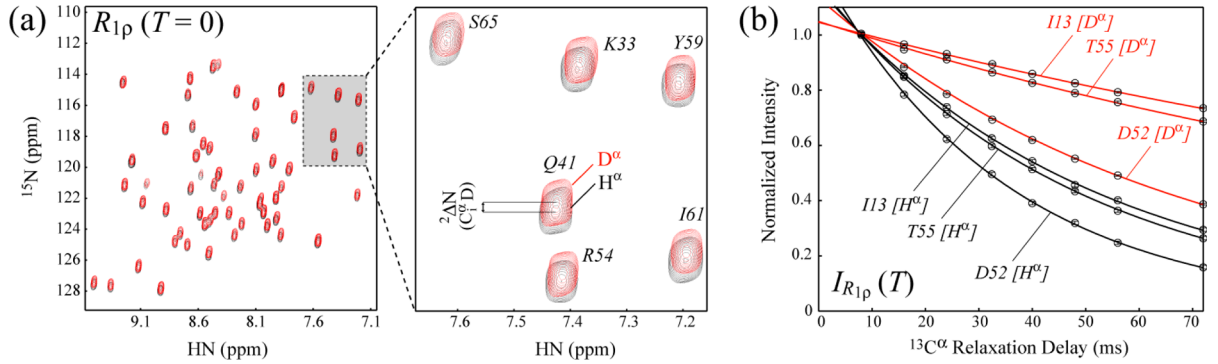

Figure 4. (a) Superposition of a region of the 2D *intra*-HN[CA] correlation maps corresponding to the first point of $R_{1\rho}$ measurements (relaxation delay T = 0 in Figure 1) in $^{13}C^{\alpha}$–H^{α} (black contours) and $^{13}C^{\alpha}$–D^{α} (red contours) spin pairs. Displacements in peak positions result from the two-bond deuterium isotope shift, $^{2}\Delta N(C^{\alpha,i}D)$. (b) Selected $^{13}C^{\alpha}$ $R_{1\rho}$ relaxation decays obtained with the 2D *intra*-HN[CA] experiment in $^{13}C^{\alpha}$–H^{α} (black curves) and $^{13}C^{\alpha}$–D^{α} (red curves) spin pairs of Ile,[13] Thr,[55] and Asp[52] of ubiquitin (600 MHz, 27 °C).

relaxation rates are interpreted to extract the parameters of local dynamics. In practice, it may be difficult to account for all these contributions quantitatively because of the uncertainties in the order parameters of the involved interactions, internuclear distances, residue-specific $^{13}C^{\alpha}$ CSA values, and chemical exchange contributions. For example, in our recent $^{13}C^{\alpha}$ relaxation study on the [$^{13}C^{\alpha}$]-labeled ubiquitin, the r_{CH} distance of 1.09 Å had to be used to achieve quantitative agreement between the spin relaxation-derived order parameters S^2 and those obtained from the 1 μs MD simulation.[37] The use of the shorter distance uniformly lowers the derived $^{13}C^{\alpha}$–H^{α} S^2 by ~6% effectively "absorbing" all the contributions to relaxation rates that remain unaccounted for even in the most careful of analyses. Below, we show that differential $^{13}C^{\alpha}$ R_1 and R_2 rates measured in $^{13}C^{\alpha}$–H^{α} and $^{13}C^{\alpha}$–D^{α} spin pairs of a partially deuterated U-[^{13}C]-labeled protein serve as reliable, "external" interaction-, CSA-, and chemical exchange-free measures of local dynamics at α-carbon sites of proteins.

Measurements of α-Carbon R_1 and R_2 Spin Relaxation Rates in $^{13}C^{\alpha}$–H^{α} and $^{13}C^{\alpha}$–D^{α} Spin Pairs of Ubiquitin. The 2D *intra*-HN[CA] experiment[84,85] developed for the measurement of $^{13}C^{\alpha}$ $R_{1\rho}$ and R_1 relaxation rates in $^{13}C^{\alpha}$–H^{α} and $^{13}C^{\alpha}$–D^{α} spin pairs of proteins (Figure 1) is of the "*out-and-other-way-back*" variety.[86] The flow of magnetization in the "preparation" part of the scheme is represented by

$$H_{tr}^{N,i} \rightarrow 2H_z^{N,i}N_z^i(a) \rightarrow 8N_z^iC_z^{\alpha,i}C_z^{\alpha,i-1}C_z^{\prime,i-1}(b) \rightarrow 4N_z^i C_z^{\alpha,i}C_z^{\prime,i-1}(c) \rightarrow 2N_z^iC_z^{\alpha,i}(d) \quad (3)$$

where the signs are omitted; the subscript "tr" denotes transverse magnetization; and the letters in parentheses (a–d) correspond to the time points labeled in Figure 1 (see also the scheme in Figure 2). After the time point d in the scheme, the magnetization is filtered for either $^{13}C^{\alpha}$–H^{α} or $^{13}C^{\alpha}$–D^{α} spin pairs ($C^{\alpha}D_2$ in glycines) via the BIRD[38,39] element $\boldsymbol{F}$ followed by the measurements of $^{13}C^{\alpha}$ relaxation rates R_1 (inset $\boldsymbol{A}$) and $R_{1\rho}$ (inset $\boldsymbol{B}$) in spin pairs of each type. Note that what is effectively measured are the R_1 and $R_{1\rho}$ rates of the magnetization terms $2N_z^iC_z^{\alpha,i}$ and $2N_z^iC_{tr}^{\alpha,i}$, respectively. The transfer of magnetization back to amide protons for detection is combined with the

dx.doi.org/10.1021/jp312292k | J. Phys. Chem. B 2013, 117, 1308–1320

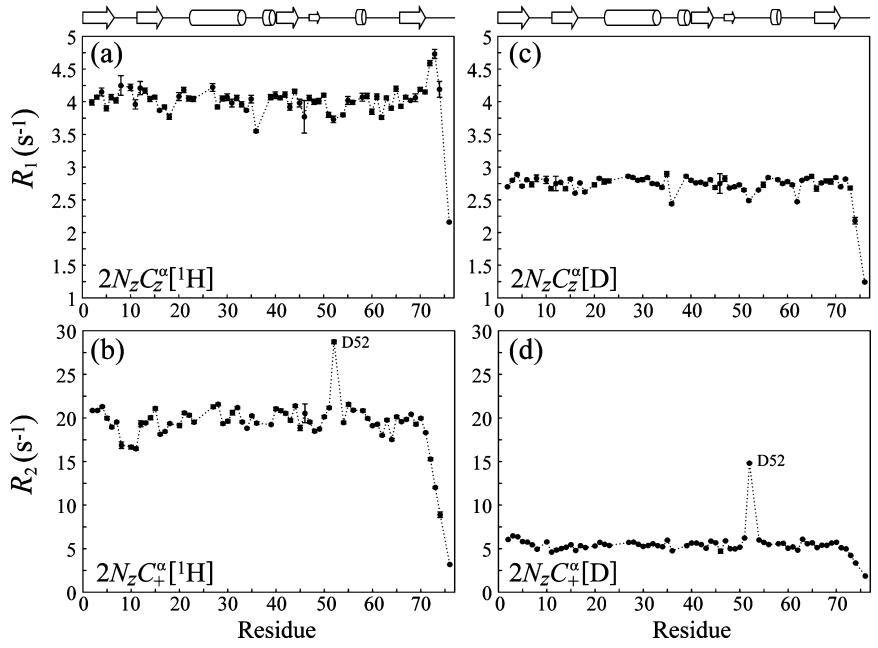

Figure 5. $^{13}C^\alpha$ relaxation rates (s^{-1}) measured in $^{13}C^\alpha$–H^α and $^{13}C^\alpha$–D^α spin pairs of ubiquitin at 27 °C plotted as a function of ubiquitin residue numbers: (a) $^{13}C^\alpha$ R_1 and (b) $^{13}C^\alpha$ R_2 in $^{13}C^\alpha$–H^α pairs; (c) $^{13}C^\alpha$ R_1 and (d) $^{13}C^\alpha$ R_2 in $^{13}C^\alpha$–D^α pairs. The magnetization terms evolving during the relaxation delay T in the experiment of Figure 1 are indicated on the plots. Schematic diagram of the secondary structure is shown above the figure.

evolution of $^{15}N^i$ chemical shift during t_1 and uses a shorter pathway via refocusing of intraresidual one-bond J couplings, $^1J_{NC\alpha}$.

A superposition of a region of the 2D *intra*-HN[CA] correlation maps corresponding to the first point of $R_{1\rho}$ measurements (relaxation delay T = 0) in $^{13}C^\alpha$–H^α (black contours) and $^{13}C^\alpha$–D^α (red contours) spin pairs is shown in Figure 4a. Displacements in peak positions result from the $^1H \rightarrow D$ substitution at α-carbon sites—a two-bond deuterium isotope shift, $^2\Delta N(C^{\alpha,i}D)$. Detailed analysis of the $^2\Delta N(C^{\alpha,i}D)$ shifts in ubiquitin in terms of backbone geometry has been reported in our previous publication.[27] All $^2\Delta N(C^{\alpha,i}D)$ shifts are positive (if defined as $^2\Delta N(C^{\alpha,i}D) = \delta N(H^{\alpha,i}) - \delta N(D^{\alpha,i})$) and vary from 70 to 220 ppb. Note that the three-bond isotope shifts resulting from ^{1}H-to-D substitution at C^α positions of residue $i-1$ and C^β sites of residue i, $^3\Delta N(C^{\alpha,i-1}D)$ and $^3\Delta N(C^{\beta,i}D)$ (see Figure 2), remain unresolved in the 2D *intra*-HN[CA] correlation maps obtained with the scheme of Figure 1. Figure 4b shows selected $^{13}C^\alpha$ $R_{1\rho}$ relaxation decays obtained using the 2D *intra*-HN[CA] scheme in $^{13}C^\alpha$–H^α (black curves) and $^{13}C^\alpha$–D^α (red curves) spin pairs of a number of residues of ubiquitin at 27 °C. $^{13}C^\alpha$ relaxation rates measured in $^{13}C^\alpha$–H^α and $^{13}C^\alpha$–D^α spin pairs at 27 °C are plotted versus residue numbers in Figure 5: R_1 (5a), R_2 (5b) in $^{13}C^\alpha$–H^α pairs and R_1 (5c), R_2 (5d) in $^{13}C^\alpha$–D^α pairs, while the plots of $^{13}C^\alpha$ relaxation rates measured at 10 °C are provided in Figure S2 of the Supporting Information. Clearly, due to the reduced strength of the dipolar interaction of α-carbon with the directly attached nucleus in $^{13}C^\alpha$–D^α spin pairs, both R_1 and R_2 rates are lower in deuterated carbon sites. The contribution of chemical exchange to the R_2 rates of Asp[52] in both types of spin pairs is also evident from the plots in Figure 5b,d ($R_{ex} \approx 8$ s^{-1}). Asp[52] is a part of a 7-residue loop in the structure of ubiquitin,[61] and its amide is hydrogen bonded to water molecules. Of note, the amide correlation of the following residue, Gly,[53] is usually very weak in [^{1}H–^{15}N] correlation maps of ubiquitin.

Earlier, Yamazaki et al.[33] and Engelke and Rüterjans[75,76] analyzed the possibility of Hartmann–Hahn magnetization transfer[83] during the spin-lock periods of $^{13}C^\alpha$ $R_{1\rho}$ measurements in U-[^{13}C]-labeled protein samples. For the ^{13}C spin-lock field strength of 2 kHz used in this study, the Hartmann–Hahn effects are negligible with the exception of certain serine and (occasionally) threonine residues where the differences between $^{13}C^\alpha$ and $^{13}C^\beta$ chemical shifts can be sufficiently small to compromise $R_{1\rho}$ measurements.[33] In ubiquitin, there is only one serine residue, Ser,[57] with very similar $^{13}C^\alpha$ and $^{13}C^\beta$ chemical shifts −61.1 and 62.5 ppm, respectively. Its cross-peak partially overlaps with that of Asp[39] in 2D *intra*-HN[CA] maps and had to be in any case excluded from analysis.

Longitudinal relaxation of the terms $N_zC_z^\alpha[H^\alpha]$ and $N_zC_z^\alpha[D^\alpha]$ during the delay T of the experiment in Figure 1 is multiexponential and can be described for either spin pair by

$$\frac{d}{dT}\begin{pmatrix}\Delta N_zC_z^\alpha\\ \Delta N_zC_z^\beta\\ \Delta N_zC_z'\end{pmatrix} = -\begin{bmatrix}\rho_{C\alpha} & \sigma_{\alpha,\beta} & \sigma_{\alpha,'}\\ \sigma_{\alpha,\beta} & \rho_{C\beta} & 0\\ \sigma_{\alpha,'} & 0 & \rho_{C'}\end{bmatrix}\begin{pmatrix}\Delta N_zC_z^\alpha\\ \Delta N_zC_z^\beta\\ \Delta N_zC_z'\end{pmatrix} \quad (4)$$

where $\Delta N_zC_z^i(T) = N_zC_z^i(T,\uparrow) - N_zC_z^i(T,\downarrow)$ with $N_zC_z^i(T,\uparrow)$ and $N_zC_z^i(T,\downarrow)$ denoting the z component of $N_zC_z^i$ magnetization for the initial state of the carbon magnetization ($T = 0$) aligned along the $+Z$ or the $-Z$ axis, respectively, while ρ_{Ci} and $\sigma_{i,j}$ denote the auto- and cross-relaxation rates of carbon spins[33,75,76,87−89] (i = α, β, $'$; see the scheme in Figure 2). Exact expressions for the relaxation rates ρ and σ can be found, for example, in Yamazaki et al.[33] Note that the relaxation rate of the $N_zC_z^\alpha$ term does not depend on the equilibrium carbon magnetization by virtue of the phase-cycling of the ^{13}C pulse with phase $\phi4'$ together with the phase of the receiver (Figure 1, inset *A*),[90] while cross-relaxation with $^1H^\alpha$ spins is eliminated by ^{1}H pulses applied during the relaxation delay T.

For small values of $(\sigma_{i,j}/\rho_{Ci})$ the evolution of $\Delta N_zC_z^\alpha$ can be to a very good approximation described using perturbation

dx.doi.org/10.1021/jp312292k | J. Phys. Chem. B 2013, 117, 1308−1320

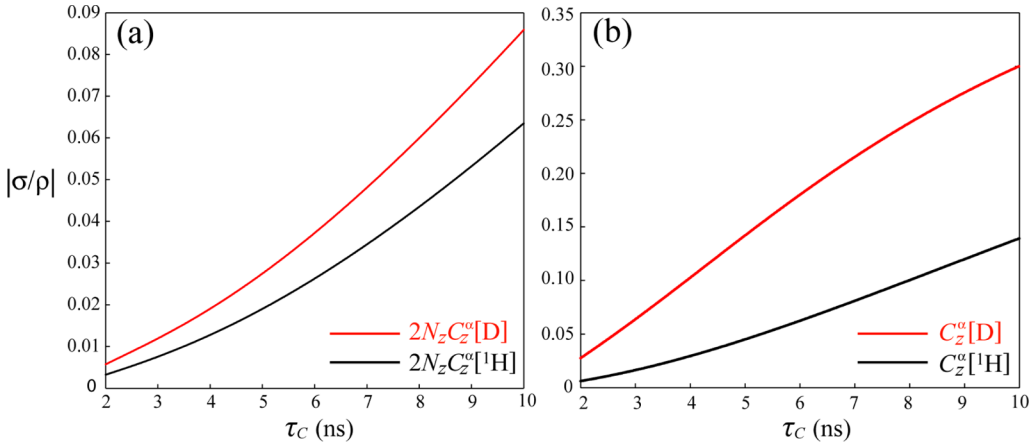

Figure 6. Plots of the calculated absolute ratio of auto- and cross-relaxation rates, $|\sigma/\rho|$, as a function of the isotropic global molecular rotational correlation time, τ_C, for $^{13}C^\alpha$–H^α (black curves) and $^{13}C^\alpha$–D^α (red curves) spin pairs. (a) $|\sigma/\rho|$ calculated for the auto-(ρ) rates of the $N_zC_z^\alpha$ magnetization terms (quantified in the experiment of Figure 1) vs τ_C. (b) $|\sigma/\rho|$ calculated for the auto-(ρ) rates of the C_z^α magnetization terms only (longitudinal ^{15}N relaxation excluded). All calculations have been performed using the parameters of local dynamics of C^α–H^α(D^α) bond vectors: S^2 = 0.9 and τ_f = 20 ps.

treatment.[33] For initial conditions $\Delta N_zC_z^\beta(0) = \Delta N_zC'(0) = 0$ and assuming $\sigma_{\alpha,\beta} = \sigma_{\alpha,'} = \sigma$, the evolution of $\Delta N_zC_z^\alpha(T)$ can be approximated to second order by[33]

$$\Delta N_zC_z^\alpha(T) \cong \Delta N_zC_z^\alpha(0)\exp(-\rho_{C\alpha}T)+ \Delta N_zC_z^\alpha(0)\left\{\begin{aligned}&\left[\frac{\sigma}{(\rho_{C\alpha}-\rho_{C\beta})}\right]^2[\exp(-\rho_{C\beta}T)-\exp(-\rho_{C\alpha}T)]\\ &+\left[\frac{\sigma}{(\rho_{C\alpha}-\rho_{C'})}\right]^2[\exp(-\rho_{C'}T)-\exp(-\rho_{C\alpha}T)]\\ &-\left[\frac{\sigma^2}{(\rho_{C\alpha}-\rho_{C'})}+\frac{\sigma^2}{(\rho_{C\alpha}-\rho_{C\beta})}\right]\exp(-\rho_{C\alpha}T)T\end{aligned}\right\} \quad (5)$$

We note that in the limit where $\tau_C \to \infty$ (very large proteins), $|\sigma/\rho| \to 1/2$. Yamazaki, Muhandiram, and Kay[33] have shown earlier that for proteins with global rotational correlation times τ_C below ~10 ns the absolute ratios of the cross- and autorelaxation rates, $|\sigma/\rho|$, remain sufficiently small to justify a single exponential approximation in the derivation of $^{13}C^\alpha$ R_1 rates: $\Delta N_zC_z^\alpha(T) = \Delta N_zC_z^\alpha(0)\exp(-\rho_{C\alpha}T)$. These calculations have been performed, however, for protonated proteins ($^{13}C^\alpha$–H^α spin systems), and it is not clear a priori whether the same conclusions would hold for the case of $^{13}C^\alpha$–D^α spin pairs where the (direct) dipolar contribution to $\rho_{C\alpha}$ is reduced. Figure 6a shows the plots of $|\sigma/\rho|$ as a function of τ_C for $^{13}C^\alpha$–H^α (black curves) and $^{13}C^\alpha$–D^α (red curves) spin systems, where the autorates are calculated for the $2N_zC_z^\alpha$ terms that are present during relaxation delay T in the experiment of Figure 1 (inset *A*). For τ_C of ubiquitin at 27 and 10 °C (4.16 and 6.92 ns, respectively), the ratios $|\sigma/\rho|$ in both types of spin systems remain sufficiently small to fully justify the single-exponential approximation. This result is due to the fact that longitudinal ^{15}N relaxation (N_z) contributes the bulk of $\rho_{C\alpha}$ rates in $^{13}C^\alpha$–D^α spin pairs. Figure 6b shows the $|\sigma/\rho|$ ratios calculated for the $\rho_{C\alpha}$ rates of the C_z^α term only (longitudinal ^{15}N relaxation excluded). Clearly, while the rate σ is the same in both cases (Figure 6a,b), the autorelaxation rates ρ are significantly enhanced by the relaxation rate of N_z resulting in a favorable scenario when $|\sigma/\rho|$ remain relatively small even in $^{13}C^\alpha$–D^α spin systems for τ_C values up to ~10 ns. Numerical simulations of the evolution of $\Delta N_zC_z^\alpha$ using initial conditions specified above for both $^{13}C^\alpha$–H^α and $^{13}C^\alpha$–D^α spin pairs in proteins with τ_C values up to ~10 ns using (1) exact solution obtained via the diagonalization of the relaxation matrix in eq 4 and (2) second-order perturbation expansion in eq 5 provide virtually identical $\Delta N_zC_z^\alpha(T)$ dependences largely irrespective of the assumed $\rho_{C\beta}$ and $\rho_{C'}$ rates. Furthermore, both evolution decays are practically indistinguishable from the single-exponential curves, with errors in the rates obtained from single-exponential fits well below 0.5% even in $^{13}C^\alpha$–D^α spin pairs and for the times T extending to ~$3/\rho_{C\alpha}$.

One-bond $^{13}C^\alpha$–H^α scalar couplings, $^1J_{C\alpha-H\alpha}$, are not as uniform as $^1J_{NH}$ couplings in proteins and vary between 134 and 151 Hz in ubiquitin.[27,91] This variation might potentially compromise the selection for $^{13}C^\alpha$–D^α spin pairs in the experiment of Figure 1 since the admixture of even a small amount of (fast-relaxing) $^{13}C^\alpha$–H^α species may significantly affect the extracted rates. The proportion of the intensity "leakage" from $^{13}C^\alpha$–H^α spin pairs relative to the intensity of $^{13}C^\alpha$–D^α species, I_{CH}, in the experiment of Figure 1 is calculated to be given by

$$I_{CH} = \frac{1}{2}\left(\frac{N_{CH}}{N_{CD}}\right)[1+\cos(4\pi^1J_{C\alpha-H\alpha}\tau_d)] \times \exp\{4(R_2[C^\alpha D]-R_2[C^\alpha H])\tau_d\} \quad (6)$$

where N_{CH}/N_{CD} is the ratio of the abundances of $^{13}C^\alpha$–H^α and $^{13}C^\alpha$–D^α pairs in the protein sample (2/3 for a [40%-^{1}H/60%-^{2}H] sample used here). For an average value of $^1J_{C\alpha-H\alpha}$ = 143 Hz (used for the calculation of delays τ_d in the filter element *F*; Figure 1) I_{CH} is zero. Using eq 6 we estimate that $I_{CH} < 0.006$ even for extreme values of $^1J_{C\alpha-H\alpha}$, and the $^{13}C^\alpha$–D^α rates are not affected by this contribution to within experimental errors. We note that the relative contributions of ^{13}CHD and $^{13}CH_2$ species to the $^{13}CD_2$ filtering in glycines ("CD_2" element in Figure 1) are proportional to $\cos(2\pi^1J_{C\alpha-H\alpha}\tau_d)$ and $\cos^2(2\pi^1J_{C\alpha-H\alpha}\tau_d)$ (assuming the same $^1J_{C\alpha-H\alpha}$ for the two $^{13}C^\alpha$–H^α couplings), respectively, leading to substantially higher I_{CH} for these residues in the cases when at least one of the Gly $^1J_{C\alpha-H\alpha}$ deviates from 143 Hz by more than ~4 Hz. Therefore, the margin of error in

dx.doi.org/10.1021/jp312292k | J. Phys. Chem. B 2013, 117, 1308–1320

the extracted rates for $^{13}CD_2$ groups in glycines may be much higher than for the rest of the residues.

Differential R_1, R_2 Relaxation in $^{13}C^{\alpha}$–H^{α}/$^{13}C^{\alpha}$–D^{α} Spin Pairs. As all the "external" contributions to $^{13}C^{\alpha}$ relaxation rates in U-[^{13}C] proteins described above, including $^{13}C^{\alpha}$ CSA and chemical exchange, are the same for $^{13}C^{\alpha}$–H^{α} and $^{13}C^{\alpha}$–D^{α} spin pairs, in lieu of interpreting $^{13}C^{\alpha}$ relaxation data of each individual spin system separately in terms of parameters of local motions (S^2 and τ_f), we pursue an obviously much more attractive alternative and calculate the differences between the corresponding $^{13}C^{\alpha}$ R_1 and R_2 rates: $\Delta R_2 = R_2[^{13}C^{\alpha}–H^{\alpha}] - R_2[^{13}C^{\alpha}–D^{\alpha}]$ and $\Delta R_1 = R_1[^{13}C^{\alpha}–H^{\alpha}] - R_1[^{13}C^{\alpha}–D^{\alpha}]$. ΔR_2 is to a good approximation described by

$$\begin{aligned} &R_2(N_zC_+^{\alpha}[^1H]) - R_2(N_zC_+^{\alpha}[D]) \\ &= \frac{1}{4}\left(\frac{\mu_0}{4\pi}\right)^2\left(\frac{\gamma_H\gamma_C\hbar}{r_{CH}^3}\right)^2\begin{bmatrix}4J(0) + J(\omega_H - \omega_C) + 3J(\omega_C)\\ + 6J(\omega_H) + 6J(\omega_H + \omega_C)\end{bmatrix} \\ &\quad - \frac{2}{3}\left(\frac{\mu_0}{4\pi}\right)^2\left(\frac{\gamma_D\gamma_C\hbar}{r_{CD}^3}\right)^2\begin{bmatrix}4J(0) + J(\omega_C - \omega_D) + 3J(\omega_C)\\ + 6J(\omega_D) + 6J(\omega_D + \omega_C)\end{bmatrix} \end{aligned} \quad (7a)$$

where μ_0 is the vacuum permeability constant; γ_i is the gyromagnetic ratio of spin i; r_{lk} is the distance between nuclei l and k; and $J(\omega)$ is the spectral density function evaluated at the frequency ω (eq 2). In the single-exponential approximation justified in the previous section, the differential R_1 rate, ΔR_1, is given by

$$\begin{aligned} &R_1(N_zC_z^{\alpha}[^1H]) - R_1(N_zC_z^{\alpha}[D]) \\ &= \frac{1}{2}\left(\frac{\mu_0}{4\pi}\right)^2\left(\frac{\gamma_H\gamma_C\hbar}{r_{CH}^3}\right)^2\begin{bmatrix}J(\omega_H - \omega_C) + 3J(\omega_C)\\ + 6J(\omega_H + \omega_C)\end{bmatrix} \\ &\quad - \frac{4}{3}\left(\frac{\mu_0}{4\pi}\right)^2\left(\frac{\gamma_D\gamma_C\hbar}{r_{CD}^3}\right)^2\begin{bmatrix}J(\omega_C - \omega_D) + 3J(\omega_C)\\ + 6J(\omega_D + \omega_C)\end{bmatrix} \end{aligned} \quad (7b)$$

Note that ^{13}C R_1 and R_2 rates in $^{13}C^{\alpha}$–H^{α} and $^{13}C^{\alpha}$–D^{α} spin systems in eqs 7a and 7b are proportional to $S(S + 1)$, where S is the spin quantum number of a proton ($S = 1/2$) or a deuteron ($S = 1$) ensuring that $^{13}C^{\alpha}$ rates in $^{13}C^{\alpha}$–D^{α} spin systems have a prefactor 8/3 larger than that for the rates in $^{13}C^{\alpha}$–H^{α} spin pairs. In glycine residues, the differential rates in eqs 7a and 7b describe the differences between $^{13}C^{\alpha}$ relaxation rates in $^{13}C^{\alpha}HD$ and $^{13}C^{\alpha}D_2$ moieties where the contribution of one deuteron is always subtracted in the isotropic approximation for $J(\omega)$ (see Materials and Methods).

Equations 7a and 7b describing differential relaxation rates ΔR_1 and ΔR_2 are approximate because the longitudinal ^{15}N (N_z) relaxation rate of ^{15}N spins attached to $^{13}C^{\alpha}$–H^{α} or $^{13}C^{\alpha}$–D^{α} spin pairs is slightly different. Therefore, both ΔR_1 and ΔR_2 include an additional term arising from the fact that $R_1(N_z[^1H^{\alpha}]) \neq R_1(N_z[D^{\alpha}])$

$$\begin{aligned} &R_1(N_z[^1H^{\alpha}]) - R_1(N_z[D^{\alpha}]) \\ &= \frac{1}{2}\left(\frac{\mu_0}{4\pi}\right)^2\left(\frac{\gamma_H\gamma_N\hbar}{r_{NH^{\alpha}}^3}\right)^2\begin{bmatrix}J(\omega_H - \omega_N) + 3J(\omega_N)\\ + 6J(\omega_H + \omega_N)\end{bmatrix} \\ &\quad - \frac{4}{3}\left(\frac{\mu_0}{4\pi}\right)^2\left(\frac{\gamma_D\gamma_N\hbar}{r_{ND^{\alpha}}^3}\right)^2\begin{bmatrix}J(\omega_D - \omega_N) + 3J(\omega_N)\\ + 6J(\omega_D + \omega_N)\end{bmatrix} \end{aligned} \quad (8)$$

The contribution of this difference to ΔR_1 and ΔR_2 is estimated to be 0.1(0.04%) for ΔR_2 in ubiquitin at 27(10) °C and 1.1% for ΔR_1 at both temperatures using $r_{NH^{\alpha}} = r_{ND^{\alpha}} = 2.10$ Å. Although it is practically negligible and within experimental errors in ΔR_1 and ΔR_2 for most of the $^{13}C^{\alpha}$ sites in ubiquitin, the difference in eq 8 has been included for completeness in all calculations of differential rates.

Figure 7 shows the differential $^{13}C^{\alpha}$ relaxation rates ΔR_1 (Figure 7a) and ΔR_2 (Figure 7b) obtained in ubiquitin at

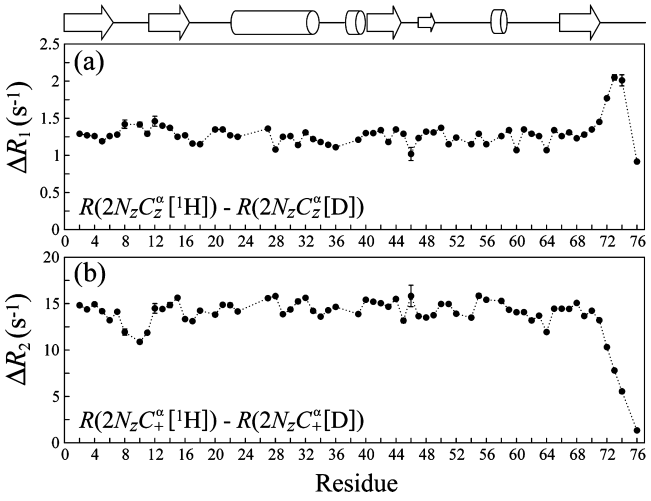

Figure 7. Differential $^{13}C^{\alpha}$ relaxation rates (s^{-1}) obtained in ubiquitin at 27 °C plotted versus residue numbers: (a) $\Delta R_1 = R_1[^{13}C^{\alpha}–H^{\alpha}] - R_1[^{13}C^{\alpha}–D^{\alpha}]$ and (b) $\Delta R_2 = R_2[^{13}C^{\alpha}–H^{\alpha}] - R_2[^{13}C^{\alpha}–D^{\alpha}]$. Schematic diagram of the secondary structure of ubiquitin is shown above the figure.

27 °C plotted versus residue numbers, while the same plots at 10 °C are provided in Figure S3 of the Supporting Information. The contributions to $^{13}C^{\alpha}$ R_1 relaxation rates arising from homonuclear $^{13}C^{\alpha}$–$^{13}C^{\beta}$ and $^{13}C^{\alpha}$–$^{13}C'$ dipolar interactions, heteronuclear dipolar interactions with ^{15}N and external ^1H spins, as well as $^{13}C^{\alpha}$ CSA relaxation are subtracted out from ΔR_1 and ΔR_2 rates. The profile of ΔR_2 rates distinguishes the flexible loop Leu^8-Lys^{11} and the C-terminal residues Arg^{72}-Gly^{76} in ubiquitin with lower than average ΔR_2 (Figure 7b). The most remarkable feature of the plot in Figure 7b is the elimination of the chemical exchange contribution to the R_2 rates in Asp^{52} clearly identifiable in Figures 3b,d and 5b,d.

Dynamics of $^{13}C^{\alpha}$–$H^{\alpha}(D^{\alpha})$ Bond Vectors from the Differences in R_1, R_2 Relaxation Rates in $^{13}C^{\alpha}$–H^{α} and $^{13}C^{\alpha}$–D^{α} Spin Pairs. Earlier, Skrynnikov, Kay, and co-workers reported NMR measurements and analysis of ^{15}N relaxation data in ^{15}N–^1H and ^{15}N–D spin pairs of proteins using a protonated sample of protein L dissolved in 50% H_2O/50% D_2O.[26] Spectral density mapping[92] applied to differential relaxation rates ΔR_1 and ΔR_2 in ^{15}N–^1H/^{15}N–D spin pairs obtained at two spectrometer fields allowed evaluation of the contributions of the spectral density function sampled at a uniquely low frequency, $J(\omega_D + \omega_N)$ (31 MHz at a 600 MHz spectrometer field), inaccessible using conventional nuclear probes of protein dynamics. However, in the case of $^{13}C^{\alpha}$–D^{α} spin pairs, the analogous spectral density terms would involve the frequency $(\omega_C - \omega_D)$, $J(\omega_C - \omega_D)$ in eqs 7a and 7b, equal to 59 MHz at a 600 MHz spectrometer field, which is very close to the frequency of ^{15}N (61 MHz) and therefore is not a unique reporter of local motions on the nanosecond time scale. On the other hand, while the

dx.doi.org/10.1021/jp312292k | J. Phys. Chem. B 2013, 117, 1308–1320

measurements of ^{15}N relaxation in $^{15}N-D$ spin pairs by direct nitrogen detection conducted by Fushman and co-workers[25] provided useful information about the magnitude and orientation of amide ^{15}N CSA tensors due to the reduced relative contribution of the dipolar relaxation in these spin systems,[25] because of the small magnitude of $^{13}C^{\alpha}$ CSA this approach is not applicable to $^{13}C^{\alpha}-D^{\alpha}$ pairs. That is why we have chosen to extract the parameters of local motions (S^2 and τ_f) from direct best fits of differential ΔR_1 and ΔR_2 rates (eqs 7a and 7b) to model-free[58,59] expressions for the spectral density function in eq 2 (except glycines where isotropic approximation for $J(\omega)$ was used; see Materials and Methods) under the working assumption that the local dynamics parameters of $C^{\alpha}-H^{\alpha}$ and $C^{\alpha}-D^{\alpha}$ bond vector motions are the same, i.e., not significantly affected by the ^1H-to-D substitution at α-carbon sites. This is deemed to be a reasonable surmise because the change in the nuclear mass of 1 a.m.u. resulting from ^1H-to-D substitution is small relative to the total mass of a $^{13}C-^1H(D)$ spin pair. As ^{13}C dipolar spin relaxation in $^{13}C-H$ and $^{13}C-D$ moieties is also affected by local vibrational motions, we conducted an approximate quantum-mechanical analysis of the effects of zero-point vibrations on spin relaxation[93−95] in $^{13}C-H$ and $^{13}C-D$ pairs considering one stretching and two bending vibrational modes (see Supporting Information). We find that in the case of an axially symmetric potential the effects of stretching and bending motions nearly cancel each other (Table S1 of the Supporting Information). More detailed treatment of the effects of ^1H-to-D substitution on the order parameters would involve the consideration of additional librational modes as described earlier for proteins[93,96] and a peptide fragment.[94]

We compare the (ΔR_1, ΔR_2)-derived measures of order with their counterparts derived from $^{13}C^{\alpha}$ relaxation measurements conducted on selectively [$^{13}C^{\alpha}$]-labeled samples of ubiquitin[37] and those derived from MD simulations. Figure 8a compares the (ΔR_1, ΔR_2)-derived generalized order parameters S^2 of $C^{\alpha}-H^{\alpha}(D^{\alpha})$ bond vector motions in ubiquitin with S^2 derived from the 500 ns MD trajectories at 27 °C. Although the overall agreement in S^2 variation patterns is quite remarkable, the absolute agreement is somewhat inferior to the one reported previously between ($^{13}C^{\alpha}$ R_1, R_2)-derived S^2 in the [$^{13}C^{\alpha}$]-labeled ubiquitin and the MD simulation.[37] Notably, (ΔR_1, ΔR_2)-derived S^2 tend to be uniformly lower than their MD-derived counterparts. Figure 8b compares the $^{13}C^{\alpha}$ (ΔR_1, ΔR_2)-derived S^2 with those obtained from analysis of ($^{13}C^{\alpha}$ R_1, R_2) relaxation rates measured in the selectively [$^{13}C^{\alpha}$]-labeled protein sample. Clearly, some unaccounted contributions to $^{13}C^{\alpha}$ relaxation rates in the [$^{13}C^{\alpha}$]-labeled protein (primarily to R_2 rates in the case of S^2 comparisons) drive S^2 to the values which are uniformly higher (by ~0.05 on average) than their (ΔR_1, ΔR_2)-derived counterparts, with some of the ($^{13}C^{\alpha}$ R_1, R_2)-derived measures of order close to or exceeding the theoretical S^2 maximum of ~0.95 ($S \approx 0.975$) (Figure 8b). Although comparisons of *absolute* measures of order obtained using different experimental/computational techniques and protein samples may be problematic, we feel it is warranted in this case, as the S^2 values are derived using identical parameters of global motion (see Materials and Methods) and the same effective r_{CH} distance of 1.10 Å. The (ΔR_1, ΔR_2)-derived time scales of $C^{\alpha}-H^{\alpha}(D^{\alpha})$ bond vector dynamics, τ_f, are plotted in Figure 8c. The regions with slower motions (higher τ_f values) generally coincide with the regions of the molecule lacking defined secondary structure: the loops Leu[8]-Lys,[11] Leu[50]-Leu,[56] and the C-terminal residues.

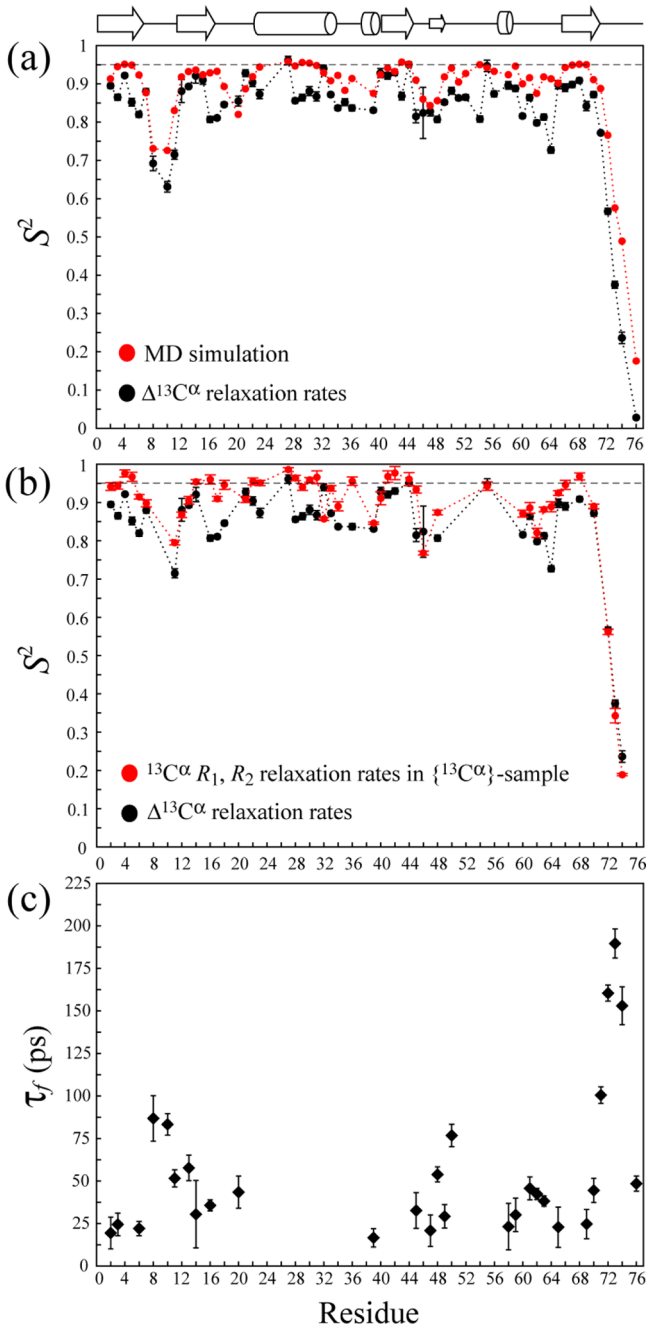

Figure 8. Plots of the generalized order parameter,[58,59] S^2, of $C^{\alpha}-H^{\alpha}(D^{\alpha})$ bond vector motions in ubiquitin derived from: (a) differential $^{13}C^{\alpha}$ rates ΔR_1, ΔR_2 (black circles) and molecular dynamics simulation at 27 °C (red circles); (b) differential $^{13}C^{\alpha}$ rates ΔR_1, ΔR_2 (black circles) and $^{13}C^{\alpha}$ R_1, R_2 relaxation rates measured in the selectively [$^{13}C^{\alpha}$]-labeled ubiquitin (red circles) at 27 °C. (c) The values of the time scale of $C^{\alpha}-H^{\alpha}(D^{\alpha})$ bond vector motions, τ_f (ps), obtained from the differential rates ΔR_1, ΔR_2 in ubiquitin at 27 °C. The horizontal dashed line in (a-b) is drawn at $S^2 = 0.95$, the approximate theoretical maximum for S^2 of fast librational motions. All S^2 and τ_f parameters are derived using the distance r_{C-H} of 1.10 Å and plotted versus residue numbers. A diagram of the secondary structure of ubiquitin is shown above the figure.

A similar analysis of $^{13}C^{\alpha}$ relaxation rates in ubiquitin at 10 °C is provided in Figure S4 of the Supporting Information. While, as expected, the set of $^{13}C^{\alpha}$ (ΔR_1, ΔR_2)-derived S^2 at 10 °C is uniformly higher than S^2 derived at 27 °C with rare exceptions

dx.doi.org/10.1021/jp312292k | J. Phys. Chem. B 2013, 117, 1308−1320

(Figure S4a, Supporting Information), the trend showing generally lower $^{13}C^{\alpha}$ (ΔR_1, ΔR_2)-derived S^2 in comparison to the values obtained from the selectively [$^{13}C^{\alpha}$]-labeled protein is preserved at 10 °C (Figure S4b, Supporting Information). We note that the use of the r_{CH} distance of 1.10 Å leads to a number of residues in the [$^{13}C^{\alpha}$]-labeled protein with S^2 near or above unity, indicating that some contributions to $^{13}C^{\alpha}$ transverse relaxation rates remain unaccounted for.

Concluding Remarks. In summary, we introduce NMR methodology for the measurements of α-carbon R_1 and $R_{1\rho}$ spin relaxation rates in $^{13}C^{\alpha}-H^{\alpha}$ and $^{13}C^{\alpha}-D^{\alpha}$ spin pairs of U-[^{13}C;^{15}N] partially deuterated proteins. The developed *intra*-HN[CA] NMR experiment selects for carbon nuclei of either $^{13}C^{\alpha}-H^{\alpha}$ or $^{13}C^{\alpha}-D^{\alpha}$ spin systems in the same protein sample prior to the measurement of $^{13}C^{\alpha}$ relaxation rates. The differences between R_1 and R_2 rates in the two spin pairs (ΔR_1, ΔR_2) eliminate all contributions to $^{13}C^{\alpha}$ relaxation rates that are not associated with (direct) $^{13}C^{\alpha}-^{1}H^{\alpha}(D^{\alpha})$ dipolar interactions, including chemical exchange, and serve as robust probes of $C^{\alpha}-H^{\alpha}(D^{\alpha})$ bond vector motions in proteins. The methodology is applied to the relaxation study of α-carbon sites in the protein ubiquitin at two temperatures assuming that the local dynamics is not affected by $^{1}H^{\alpha}$-to-D^{α} substitutions.

We estimate that *intra*-HN[CA] relaxation measurements performed with selection for $^{13}C^{\alpha}-H^{\alpha}$ spin pairs are on average ~4.5 times less sensitive than the measurements of $^{13}C^{\alpha}$ relaxation using $^{1}H-^{13}C$ NMR spectroscopy on U-[^{13}C]-labeled samples[33] at 27 °C. This factor includes the losses associated with partial deuteration (i.e., only 40% of the molecules in the sample used in this work contain α-protons). If the percentage of deuteration is taken into account, the sensitivity losses are reduced to a factor of only ~1.8 on average. This relatively small decrease in sensitivity is in part a consequence of the fact that ^{15}N transverse magnetization is present during most of the transfer steps of the scheme in Figure 1, whereas 2D $^{1}H-^{13}C$ constant-time-(CT)-HSQC[97,98]-based scheme(s) for $^{13}C^{\alpha}$ relaxation measurements[33] involve more prolonged periods of time with $^{13}C^{\alpha}$ magnetization in the transverse plain (typically, at least for $1/^{1}J_{CC} \sim 28$ ms). Although similar sensitivity losses are observed in ubiquitin at 10 °C, the described methodology will remain applicable to relatively small molecules because for much higher molecular sizes the increasing $^{13}C-^{13}C$ cross-relaxation rates (and $|\sigma/\rho|$ ratios) will not allow reliable extraction of the R_1 rates from the fits to a single-exponential function—especially so for the $^{13}C^{\alpha}-D^{\alpha}$ spin pairs (see Figure 6).

The amplitudes of local motions of $C^{\alpha}-H^{\alpha}(D^{\alpha})$ bond vectors (S^2) derived from the fits of differential ΔR_1 and ΔR_2 rates measured in $^{13}C^{\alpha}-H^{\alpha}$ or $^{13}C^{\alpha}-D^{\alpha}$ spin pairs of ubiquitin compare well with the set of MD-simulated S^2 at 27 °C, while the measures of order obtained from the $^{13}C^{\alpha}$ (R_1, R_2) rates in the protein selectively labeled at $^{13}C^{\alpha}$ positions tend to be higher than their (ΔR_1, ΔR_2)-derived counterparts from the partially deuterated sample even though exactly the same parameters are used in the fits. Although it is the relative changes in S^2 that are of most interest in the majority of situations (e.g., resulting from ligand-binding or temperature/pressure-induced perturbations of the system), absolute values of S^2 are needed for comparing different nuclear probes of dynamics or interpreting relaxation data in terms of changes in entropy.[99−103] Finally, our approach relates relaxation-derived C−H/D S^2 values unambiguously to protein dynamics by eliminating potential contributions from modulations of C−H/D bond lengths by their environment.

■ ASSOCIATED CONTENT

Supporting Information

Figure S1 showing the dependence of α-carbon auto- and cross-relaxation rates on the isotropic global molecular rotational correlation time, τ_C, for U-[^{13}C]-labeled proteins and proteins selectively ^{13}C-labeled at α-sites. Figure S2 showing $^{13}C^{\alpha}$ R_1, R_2 rates in $^{13}C^{\alpha}-H^{\alpha}$ and $^{13}C^{\alpha}-D^{\alpha}$ spin pairs of ubiquitin at 10 °C versus residue numbers. Figure S3 plotting the differences between $^{13}C^{\alpha}$ R_1 and R_2 rates in $^{13}C^{\alpha}-H^{\alpha}$ and $^{13}C^{\alpha}-D^{\alpha}$ spin pairs of ubiquitin at 10 °C versus residue numbers. Figure S4 comparing the plots of (ΔR_1, ΔR_2)-derived S^2 in ubiquitin at 27 and 10 °C and the plots of (ΔR_1, ΔR_2)-derived S^2 with ($^{13}C^{\alpha}$ R_1, R_2)-derived S^2 at 10 °C. Also provided is a brief description of an approximate quantum-chemical treatment of the effects of ^{1}H-to-D substitution on the order parameters of C−H(D) bond vectors of proteins. This material is available free of charge via the Internet at http://pubs.acs.org.

■ AUTHOR INFORMATION

Corresponding Author

*E-mail: vitali@umd.edu. Tel.: +1-301-4051504. Fax: +1-301-3140386.

Notes

The authors declare no competing financial interest.

■ ACKNOWLEDGMENTS

The authors are grateful to Dr. Chenyun Guo (University of Maryland) for the preparation of [U−^{15}N; ^{13}C; 60%-^{2}H, 40%-^{1}H]-labeled ubiquitin. This work was supported in part by the NSF grant MCB-0918362 to R.B.

■ REFERENCES

(1) Grzesiek, S.; Anglister, J.; Ren, H.; Bax, A. ^{13}C Line Narrowing by ^{2}H Decoupling in $^{2}H/^{13}C/^{15}N$-Enriched Proteins. Applications to Triple Resonance 4D J-Connectivity of Sequential Amides. *J. Am. Chem. Soc.* **1993**, *115*, 4369−70.

(2) Farmer, B. T., II; Venters, R. Assignment of Side-Chain ^{13}C Resonances in Perdeuterated Proteins. *J. Am. Chem. Soc.* **1995**, *117*, 4187−8.

(3) Shan, X.; Gardner, K. H.; Muhandiram, D. R.; Rao, N. S.; Arrowsmith, C. H.; Kay, L. E. Assignment of ^{15}N, $^{13}C\alpha$, $^{13}C\beta$ and HN Resonances in an ^{15}N, ^{13}C, ^{2}H Labeled 64-kda Trp Repressor-Operator Complex Using Triple Resonance NMR Spectroscopy and ^{2}H-Decoupling. *J. Am. Chem. Soc.* **1996**, *118*, 6570−9.

(4) Nietlispach, D.; Clowes, R. T.; Broadhurst, R. W.; Ito, Y.; Keeler, J.; Kelly, M.; Ashurst, J.; Oschkinat, H.; Domaille, P. J.; Laue, E. D. An Approach to the Structure Determination of Larger Proteins Using Triple Resonance NMR Experiments in Conjunction with Random Fractional Deuteration. *J. Am. Chem. Soc.* **1996**, *118*, 407−15.

(5) Smith, B. O.; Ito, Y.; Raine, A.; Teichmann, S.; Ben-Tovim, L.; Nietlispach, D.; Broadhurst, R. W.; Terada, T.; Kelly, M.; Oschkinat, K.; Shibata, T.; Yokoyama, S.; Laue, E. D. An Approach to Global Fold Determination Using Limited NMR Data from Larger Proteins Selectively Protonated at Specific Residues. *J. Biomol. NMR* **1996**, *8*, 360−8.

(6) Gardner, K. H.; Rosen, M. K.; Kay, L. E. Global Folds of Highly Deuterated, Methyl Protonated Proteins by Multidimensional NMR. *Biochemistry* **1997**, *36*, 1389−401.

(7) Gardner, K. H.; Kay, L. E. The Use of ^{2}H, ^{13}C, ^{15}N Multidimensional NMR to Study the Structure and Dynamics of Proteins. *Annu. Rev. Biophys. Biomol. Struct.* **1998**, *27*, 357−406.

(8) Pervushin, K.; Riek, R.; Wider, G.; Wüthrich, K. Attenuated T_2 Relaxation by Mutual Cancellation of Dipole-Dipole Coupling and Chemical Shift Anisotropy Indicates an Avenue to NMR Structures of

Very Large Biological Macromolecules in Solution. *Proc. Natl. Acad. Sci. U.S.A.* **1997**, *94*, 12366−71.
(9) Pervushin, K. Impact of Transverse Relaxation Optimized Spectroscopy (TROSY) on NMR as a Technique in Structural Biology. *Q. Rev. Biophys.* **2000**, *33*, 161−97.
(10) Yang, D.; Kay, L. E. Improved Lineshape and Sensitivity in the HNCO-Family of Triple-Resonance Experiments. *J. Biomol. NMR* **1999**, *14*, 273−6.
(11) Pervushin, K.; Riek, R.; Wider, G.; Wüthrich, K. Transverse Relaxation-Optimized Spectroscopy for NMR Studies of Aromatic Spin Systems in ^{13}C-Labeled Proteins. *J. Am. Chem. Soc.* **1998**, *120*, 6394−400.
(12) Miclet, E.; Williams, D. C., Jr; Clore, G. M.; Bryce, D. L.; Boisbouvier, J.; Bax, A. Relaxation-Optimized NMR Spectroscopy of Methylene Groups in Proteins and Nucleic Acids. *J. Am. Chem. Soc.* **2004**, *126*, 10560−70.
(13) Tugarinov, V.; Hwang, P. M.; Ollerenshaw, J. E.; Kay, L. E. Cross-Correlated Relaxation Enhanced ^{1}H-^{13}C NMR Spectroscopy of Methyl Groups in Very High Molecular Weight Proteins and Protein Complexes. *J. Am. Chem. Soc.* **2003**, *125*, 10420−8.
(14) Tugarinov, V.; Hwang, P. M.; Kay, L. E. Nuclear Magnetic Resonance Spectroscopy of High-Molecular-Weight Proteins. *Annu. Rev. Biochem.* **2004**, *73*, 107−46.
(15) Ollerenshaw, J. E.; Tugarinov, V.; Kay, L. E. Methyl TROSY: Explanation and Experimental Verification. *Magn. Reson. Chem.* **2003**, *41*, 843−52.
(16) Tugarinov, V.; Kay, L. E. An Isotope Labeling Strategy for Methyl TROSY Spectroscopy. *J. Biomol. NMR* **2004**, *28*, 165−72.
(17) Mittermaier, A.; Kay, L. E. Effect of Deuteration on Some Structural Parameters of Methyl Groups in Proteins as Evaluated by Residual Dipolar Couplings. *J. Biomol. NMR* **2002**, *23*, 35−45.
(18) LiWang, A. C.; Bax, A. Equilibrium Protium/Deuterium Fractionation of Backbone Amides in U-^{13}C/^{15}N Labeled Human Ubiquitin by Triple Resonance NMR. *J. Am. Chem. Soc.* **1996**, *118*, 12864−5.
(19) LeMaster, D. M.; LaIuppa, J. C.; Kushlan, D. M. Differential Deuterium Isotope Shifts and One-Bond ^{1}H-^{13}C Scalar Couplings in the Conformational Analysis of Protein Glycine Residues. *J. Biomol. NMR* **1994**, *4*, 863−70.
(20) Venters, R. A.; Farmer, B. T.; Fierke, C. A.; Spicer, L. D. Characterizing the Use of Perdeuteration in NMR Studies of Large Proteins: ^{13}C, ^{15}N and ^{1}H Assignments of Human Carbonic Anhydrase II. *J. Mol. Biol.* **1996**, *264*, 1101−16.
(21) Ottiger, M.; Bax, A. An Empirical Correlation between Amide Deuterium Isotope Effects on $^{13}C^{\alpha}$ Chemical Shifts and Protein Backbone Conformation. *J. Am. Chem. Soc.* **1997**, *119*, 8070−5.
(22) Abildgaard, J.; Hansen, P. E.; Manalo, M. N.; LiWang, A. Deuterium Isotope Effects on ^{15}N Backbone Chemical Shifts in Proteins. *J. Biomol. NMR* **2009**, *44*, 119−26.
(23) Takeda, M.; Jee, J.; Terauchi, T.; Kainosho, M. Detection of the Sulfhydryl Groups in Proteins with Slow Hydrogen Exchange Rates and Determination of Their Proton/Deuteron Fractionation Factors Using the Deuterium-Induced Effects on the $^{13}C\beta$ NMR Signals. *J. Am. Chem. Soc.* **2010**, *132*, 6254−60.
(24) Maltsev, A. S.; Ying, J.; Bax, A. Deuterium Isotope Shifts for Backbone ^{1}H, ^{15}N and ^{13}C Nuclei in Intrinsically Disordered Protein α-Synuclein. *J. Biomol. NMR* **2012**, *54*, 181−191.
(25) Vasos, P. R.; Hall, J. B.; Kummerle, R.; Fushman, D. Measurement of ^{15}N Relaxation in Deuterated Amide Groups in Proteins Using Direct Nitrogen Detection. *J. Biomol. NMR* **2006**, *36*, 27−36.
(26) Xu, J.; Millet, O.; Kay, L. E.; Skrynnikov, N. R. A New Spin Probe of Protein Dynamics: Nitrogen Relaxation in ^{15}N-^{2}H Amide Groups. *J. Am. Chem. Soc.* **2005**, *127*, 3220−9.
(27) Sun, H.; Tugarinov, V. Precision Measurements of Deuterium Isotope Effects on the Chemical Shifts of Backbone Nuclei in Proteins: Correlations with Secondary Structure. *J. Phys. Chem. B* **2012**, *116*, 7436−48.
(28) Wittebort, R. J.; Rothgeb, T. M.; Szabo, A.; Gurd, F. R. Aliphatic Groups of Sperm Whale Myoglobin: ^{13}C NMR Study. *Proc. Natl. Acad. Sci. U.S.A.* **1979**, *76*, 1059−63.
(29) Richarz, R.; Nagayama, K.; Wüthrich, K. Carbon-13 Nuclear Magnetic Resonance Relaxation Studies of Internal Mobility of the Polypeptide Chain in Basic Pancreatic Trypsin Inhibitor and a Selectively Reduced Analogue. *Biochemistry* **1980**, *19*, 5189−96.
(30) Henry, G. D.; Weiner, J. H.; Sykes, B. D. Backbone Dynamics of a Model Membrane Protein: ^{13}C NMR Spectroscopy of Alanine Methyl Groups in Detergent-Solubilized M13 Coat Protein. *Biochemistry* **1986**, *25*, 590−8.
(31) Palmer, A. G.; Wright, P. E.; Rance, M. Measurement of Relaxation Time Constants for Methyl Groups by Proton-Detected Heteronuclear NMR Spectroscopy. *Chem. Phys. Lett.* **1991**, *185*, 41−6.
(32) Palmer, A. G.; Hochstrasser, R. A.; Millar, D. P.; Rance, M.; Wright, P. E. Characterization of Amino Acid Side Chain Dynamics in a Zinc-Finger Peptide Using Carbon-13 NMR Spectroscopy and Time-Resolved Fluorescence Spectroscopy. *J. Am. Chem. Soc.* **1993**, *115*, 6333−45.
(33) Yamazaki, T.; Muhandiram, R.; Kay, L. E. NMR Experiments for the Measurement of Carbon Relaxation Properties in Highly Enriched, Uniformly ^{13}C, ^{15}N Labeled Proteins: Application to $^{13}C^{\alpha}$ Carbons. *J. Am. Chem. Soc.* **1994**, *116*, 8266−78.
(34) Wand, A. J.; Urbauer, J. L.; McEvoy, R. P.; Bieber, R. J. Internal Dynamics of Human Ubiquitin Revealed by ^{13}C-Relaxation Studies of Randomly Fractionally Labeled Protein. *Biochemistry* **1996**, *35*, 6116−25.
(35) Lee, L. K.; Rance, M.; Chazin, W. J.; Palmer, A. G. Rotational Diffusion Anisotropy of Proteins from Simultaneous Analysis of ^{15}N and $^{13}C^{\alpha}$ Nuclear Spin Relaxation. *J. Biomol. NMR* **1997**, *9*, 287−98..
(36) Lundström, P.; Teilum, K.; Carstensen, T.; Bezsonova, I.; Wiesner, S.; Hansen, D. F.; Religa, T. L.; Akke, M.; Kay, L. E. Fractional ^{13}C Enrichment of Isolated Carbons Using [1-^{13}C]- or [2-^{13}C]-Glucose Facilitates the Accurate Measurement of Dynamics at Backbone C^{α} and Side-Chain Methyl Positions in Proteins. *J. Biomol. NMR* **2007**, *38*, 199−212.
(37) Sheppard, D.; Li, D. W.; Godoy-Ruiz, R.; Brüschweiler, R.; Tugarinov, V. Variation in Quadrupole Couplings of α-Deuterons in Ubiquitin Suggests the Presence of C^{α}−H^{α}···O═C Hydrogen Bonds. *J. Am. Chem. Soc.* **2010**, *132*, 7709−19..
(38) Garbow, J. R.; Weitekamp, D. P.; Pines, A. Bilinear Rotation Decoupling of Homonuclear Scalar Interactions. *Chem. Phys. Lett.* **1982**, *93*, 504−15.
(39) Meissner, A.; Briand, J.; Sørensen, O. W. Editing of Multidimensional NMR Spectra of Partially Deuterated Proteins. Measurement of Amide Deuterium Isotope Effects on the Chemical Shifts of Protein Backbone Nuclei. *J. Biomol. NMR* **1998**, *12*, 339−43.
(40) Kay, L. E.; Ikura, M.; Tschudin, R.; Bax, A. Three-Dimensional Triple-Resonance NMR Spectroscopy of Isotopically Enriched Proteins. *J. Magn. Reson.* **1990**, *89*, 496−514.
(41) Geen, H.; Freeman, R. Band-Selective Radiofrequency Pulses. *J. Magn. Reson.* **1991**, *93*, 93−141.
(42) Patt, S. L. Single- and Multiple-Frequency-Shifted Laminar Pulses. *J. Magn. Reson.* **1992**, *96*, 94−102.
(43) Boyd, J.; Soffe, N. Selective Excitation by Pulse Shaping Combined with Phase Modulation. *J. Magn. Reson.* **1989**, *85*, 406−13.
(44) Shaka, A. J.; Keeler, J.; Frenkiel, T.; Freeman, R. An Improved Sequence for Broadband Decoupling: WALTZ-16. *J. Magn. Reson.* **1983**, *52*, 335−8.
(45) Shaka, A. J.; Lee, C. J.; Pines, A. Iterative Schemes for Bilinear Operators; Application to Spin Decoupling. *J. Magn. Reson.* **1988**, *77*, 274−93.
(46) McCoy, M. A.; Mueller, L. Coherence Quenching Induced by Frequency-Selective Homonuclear Decoupling. *J. Magn. Reson.* **1992**, *98*, 674−9.
(47) Kay, L. E.; Keifer, P.; Saarinen, T. Pure Absorption Gradient Enhanced Heteronuclear Single Quantum Correlation Spectroscopy with Improved Sensitivity. *J. Am. Chem. Soc.* **1992**, *114*, 10663−5.

(48) Schleucher, J.; Sattler, M.; Griesinger, C. Coherence Selection by Gradients without Signal Attenuation: Application to the Three-Dimensional HNCO Experiment. *Angew. Chem., Int. Ed. Engl.* **1993**, *32*, 1489−91.
(49) Marion, D.; Ikura, M.; Tschudin, R.; Bax, A. Rapid Recording of 2D NMR Spectra Without Phase Cycling. Application to the Study of Hydrogen Exchange in Proteins. *J. Magn. Reson.* **1989**, *85*, 393−99.
(50) Kay, L. E.; Nicholson, L. K.; Delaglio, F.; Bax, A.; Torchia, D. A. Pulse Sequences for Removal of the Effects of Cross-Correlation between Dipolar and Chemical-Shift Anistropy Relaxation Mechanisms on the Measurement of Heteronuclear T_1 and T_2 Values in Proteins. *J. Magn. Reson.* **1992**, *97*, 359−75.
(51) Palmer, A. G.; Skelton, N. J.; Chazin, W. J.; Wright, P. E.; Rance, M. Suppression of the Effects of Cross-Correlation between Dipolar and Anisotroic Chemical Shift Relaxation Mechanisms in the Measurement of Spin-Spin Relaxation Rates. *Mol. Phys.* **1992**, *75*, 699−711.
(52) Lakomek, N. A.; Ying, J.; Bax, A. Measurement of ^{15}N Relaxation Rates in Perdeuterated Proteins by TROSY-Based Methods. *J. Biomol. NMR* **2012**, *53*, 209−21.
(53) Korzhnev, D. M.; Skrynnikov, N. R.; Millet, O.; Torchia, D. A.; Kay, L. E. An NMR Experiment for the Accurate Measurement of Heteronuclear Spin-Lock Relaxation Rates. *J. Am. Chem. Soc.* **2002**, *124*, 10743−53.
(54) Delaglio, F.; Grzesiek, S.; Vuister, G. W.; Zhu, G.; Pfeifer, J.; Bax, A. NMRPipe: A Multidimensional Spectral Processing System Based on Unix Pipes. *J. Biomol. NMR* **1995**, *6*, 277−93.
(55) Kamith, U.; Shriver, J. W. Characterization of the Thermotropic State Changes in Myosin Subfragment-1 and Heavy Meromyosin by UV Difference Spectroscopy. *J. Biol. Chem.* **1989**, *264*, 5586−92.
(56) Bevington, P. R.; Robinson, D. K. *Data Reduction and Error Analysis for the Physical Sciences*; WCB/McGraw-Hill: New York, 1992.
(57) Abragam, A. *Principles of Nuclear Magnetism*; Clarendon Press: Oxford, 1961.
(58) Lipari, G.; Szabo, A. Model-Free Approach to the Interpretation of Nuclear Magnetic Relaxation in Macromolecules: 2. Analysis of Experimental Results. *J. Am. Chem. Soc.* **1982**, *104*, 4559−70.
(59) Lipari, G.; Szabo, A. Model-Free Approach to the Interpretation of Nuclear Magnetic Relaxation in Macromolecules: 1. Theory and Range of Validity. *J. Am. Chem. Soc.* **1982**, *104*, 4546−59.
(60) Woessner, D. E. Nuclear Spin Relaxation in Ellipsoids Undergoing Rotational Brownian Motion. *J. Chem. Phys.* **1962**, *37*, 647−54.
(61) Vijay-Kumar, S.; Bugg, C. E.; Cook, W. J. Structure of Ubiquitin Refined at 1.8 Angströms Resolution. *J. Mol. Biol.* **1987**, *194*, 531−44.
(62) Sheppard, D.; Li, D. W.; Brüschweiler, R.; Tugarinov, V. Deuterium Spin Probes of Backbone Order in Proteins: A ^{2}H NMR Relaxation Study of Deuterated Carbon-α Sites. *J. Am. Chem. Soc.* **2009**, *131*, 15853−65.
(63) Raynes, W. T.; Fowler, P. W.; Lazzeretti, P.; Zanasi, R.; Grayson, M. The Effects of Rotation and Vibration on the Carbon-13 Shielding, Magnetizabilities and Geometrical Parameters of Some Methane Isotopomers. *Mol. Phys.* **1988**, *64*, 143−62.
(64) Henry, E. R.; Szabo, A. Influence of Vibrational Motion on Solid State Line Shapes and NMR Relaxation. *J. Chem. Phys.* **1985**, *82*, 4753−61.
(65) Fawcett, J. K.; Camerman, N.; Camerman, A. The Structure of the Tripeptide L-Alanyl-L-Alanyl-L-Alanine. *Acta Crystallogr.* **1975**, *B31*, 658−65.
(66) Parthasarathy, R. Crystal Structure of Glycylglycine Hydrochloride. *Acta Crystallogr.* **1969**, *B25*, 509−18.
(67) Koetzle, T. F.; Hamilton, W. C.; Parthasarathy, P. Precision Neutron Diffraction Structure Determination of Protein and Nucleic Acid Components. II. The Crystal and Molecular Structure of the Dipeptide Glycylglycine Monohydrochloride Monohydrate. *Acta Crystallogr.* **1972**, *B28*, 2083−90.
(68) Naito, A.; Ganapathy, S.; Akasaka, K.; McDowell, C. A. Chemical Shielding Tensor and ^{13}C-^{14}N Dipolar Splitting in Single-Crystals of L-Alanine. *J. Chem. Phys.* **1981**, *74*, 3190−7.
(69) Wylie, B. J.; Schwieters, C. D.; Oldfield, E.; Rienstra, C. M. Protein Structure Refinement Using $^{13}C^{\alpha}$ Chemical Shift Tensors. *J. Am. Chem. Soc.* **2009**, *131*, 985−92.
(70) Long, D.; Li, D. W.; Walter, K. F.; Griesinger, C.; Brüschweiler, R. Toward a Predictive Understanding of Slow Methyl Group Dynamics in Proteins. *Biophys. J.* **2011**, *101*, 910−5.
(71) Liao, X.; Long, D.; Li, D. W.; Brüschweiler, R.; Tugarinov, V. Probing Side-Chain Dynamics in Proteins by the Measurement of Nine Deuterium Relaxation Rates Per Methyl Group. *J. Phys. Chem. B* **2012**, *116*, 606−20.
(72) Van der Spoel, D.; Lindahl, E.; Hess, B.; Groenhof, G.; Mark, A. E.; Berendsen, H. J. GROMACS: Fast, Flexible, and Free. *J. Comput. Chem.* **2005**, *26*, 1701−18.
(73) Jorgensen, W. L.; Chandrasekhar, J.; Madura, J. D.; Impey, R. W.; Klein, M. L. Comparison of Simple Potential Functions for Simulating Liquid Water. *J. Chem. Phys.* **1983**, *79*, 926−35.
(74) Li, D. W.; Brüschweiler, R. Iterative Optimization of Molecular Mechanics Force Fields from NMR Data of Full-Length Proteins. *J. Chem. Theory Comput.* **2011**, *7*, 1773−82.
(75) Engelke, J.; Rüterjans, H. Determination of $^{13}C^{\alpha}$ Relaxation Times in Uniformly ^{13}C/^{15}N-Enriched Proteins. *J. Biomol. NMR* **1995**, *, 5*, 173−82.
(76) Engelke, J.; Rüterjans, H. In *Biological Magnetic Resonance: Structure Computation and Dynamics in Protein NMR*; N.R., K., Berliner, L. J., Eds.; Kluwer Academic/Plenum Publishers: New York, N.Y., 1999; Vol. *17*, pp 357−418.
(77) Tjandra, N.; Szabo, A.; Bax, A. Protein Backbone Dynamics and ^{15}N Chemical Shift Anisotropy from Quantitative Measurement of Relaxation Interference Effects. *J. Am. Chem. Soc.* **1996**, *118*, 6986−91.
(78) Fushman, D.; Cowburn, D. Nuclear Magnetic Resonance Relaxation in Determination of Residue-Specific ^{15}N Chemical Shift Tensors in Proteins in Solution: Protein Dynamics, Structure, and Applications of Transverse Relaxation Optimized Spectroscopy. *Methods Enzymol.* **2001**, *339*, 109−26.
(79) Hall, J. B.; Fushman, D. Variability of the ^{15}N Chemical Shielding Tensors in the B3 Domain of Protein G from ^{15}N Relaxation Measurements at Several Fields. Implications for Backbone Order Parameters. *J. Am. Chem. Soc.* **2006**, *128*, 7855−570.
(80) Yao, L.; Grishaev, A.; Cornilescu, G.; Bax, A. Site-Specific Backbone Amide ^{15}N Chemical Shift Anisotropy Tensors in a Small Protein from Liquid Crystal and Cross-Correlated Relaxation Measurements. *J. Am. Chem. Soc.* **2010**, *132*, 4295−309.
(81) Havlin, R. H.; Laws, D. D.; Bitter, H.-M. L.; Sanders, L. K.; Sun, H.; Grimley, J. S.; Wemmer, D. E.; Pines, A.; Oldfield, E. An Experimental and Theoretical Investigation of the Chemical Shielding Tensors of $^{13}C^{\alpha}$ of Alanine, Valine, and Leucine Residues in Solid Peptides and Proteins in Solution. *J. Am. Chem. Soc.* **2001**, *123*, 10362−9.
(82) Tjandra, N.; Bax, A. Large Variations in $^{13}C^{\alpha}$ Chemical Shift Anisotropy in Proteins Correlate with Secondary Structure. *J. Am. Chem. Soc.* **1997**, *119*, 9576−7.
(83) Hartmann, S. R.; Hahn, E. L. Nuclear Double Resonance in the Rotating Frame. *Phys. Rev.* **1962**, *128*, 2042−54.
(84) Permi, P. Intraresidual HNCA: An Experiment for Correlating Only Intraresidual Backbone Resonances. *J. Biomol. NMR* **2002**, *23*, 201−9.
(85) Brutscher, B. Intraresidue HNCA and COHNCA Experiments for Protein Backbone Resonance Assignment. *J. Magn. Reson.* **2002**, *156*, 155−9.
(86) Tossavainen, H.; Permi, P. Optimized Pathway Selection in Intraresidual Triple-Resonance Experiments. *J. Magn. Reson.* **2004**, *170*, 244−51.
(87) Cordier, F.; Brutscher, B.; Marion, D. Measurement of $^{13}C^{\alpha}$-^{13}CO Cross-Relaxation Rates in ^{15}N-/^{13}C-Labelled Proteins. *J. Biomol. NMR* **1996**, *7*, 163−8.
(88) Zeng, L.; Fischer, M. W. F.; Zuiderweg, E. R. P. Study of Protein Dynamics in Solution by Measurement of $^{13}C^{\alpha}$-^{13}CO NOE and ^{13}CO Longitudinal Relaxation. *J. Biomol. NMR* **1996**, *7*, 157−62.

(89) Houben, K.; Boelens, R. Side Chain Dynamics Monitored by ^{13}C-^{13}C Cross-Relaxation. *J. Biomol. NMR* **2004**, *29*, 151−66.
(90) Sklenar, V.; Torchia, D. A.; Bax, A. Measurement of Carbon-13 Longitudinal Relaxation Using ^{1}H Detection. *J. Magn. Reson.* **1987**, *73*, 375−80.
(91) Tjandra, N.; Bax, A. Measurement of Dipolar Contributions to $^{1}J_{CH}$ Splittings from Magnetic Field Dependence of J Modulation in Two-Dimensional NMR Spectra. *J. Magn. Reson.* **1997**, *124*, 512−5.
(92) Peng, J. W.; Wagner, G. Mapping of Spectral Density Functions Using Heteronuclear NMR Relaxation Measurements. *J. Magn. Reson.* **1992**, *98*, 308−32.
(93) Brüschweiler, R. Normal Modes and NMR Order Parameters in Proteins. *J. Am. Chem. Soc.* **1992**, *114*, 5341−4.
(94) Case, D. Calculations of NMR Dipolar Coupling Strengths in Model Peptides. *J. Biomol. NMR* **1999**, *15*, 95−102.
(95) Yao, L.; Vögeli, B.; Ying, J.; Bax, A. NMR Determination of Amide N−H Equilibrium Bond Length from Concerted Dipolar Coupling Measurements. *J. Am. Chem. Soc.* **2008**, *130*, 16518−20.
(96) Palmer, A. G.; Case, D. A. Molecular Dynamics Analysis of NMR Relaxation in a Zinc-Finger Peptide. *J. Am. Chem. Soc.* **1992**, *114*, 9059−67.
(97) Vuister, G. W.; Bax, A. Resolution Enhancement and Spectral Editing of Uniformly ^{13}C-Enriched Proteins by Homonuclear Broadband ^{13}C Decoupling. *J. Magn. Reson.* **1992**, *98*, 428−35.
(98) Santoro, J.; King, G. C. A Constant-Time 2D Overbodenhausen Experiment for Inverse Correlation of Isotopically Enriched Species. *J. Magn. Reson.* **1992**, *97*, 202−7.
(99) Brüschweiler, R.; Wright, P. E. NMR Order Parameters of Biomolecules: A New Analytical Representation and Application to the Gaussian Axial Fluctuation Model. *J. Am. Chem. Soc.* **1994**, *116*, 8426−7.
(100) Yang, D.; Mok, Y.-K.; Forman-Kay, J. D.; Farrow, N. A.; Kay, L. E. Contributions to Protein Entropy and Heat Capacity from Bond Vector Motions Measured by NMR Spin Relaxation. *J. Mol. Biol.* **1997**, *272*, 790−804.
(101) Lee, A. L.; Wand, A. J. Microscopic Origins of Entropy, Heat Capacity and the Glass Transition in Proteins. *Nature* **2001**, *411*, 501−4.
(102) Lee, A. L.; Kinnear, S. A.; Wand, A. J. Redistribution and Loss of Side Chain Entropy Upon Formation of a Calmodulin-Peptide Complex. *Nat. Struct. Biol.* **2000**, *7*, 72−7.
(103) Frederick, K. K.; Marlow, M. S.; Valentine, K. G.; Wand, A. J. Conformational Entropy in Molecular Recognition by Proteins. *Nature* **2007**, *448*, 325−9.